Irregular Repetition Code-Based Bit-Interleaved Coded Modulation with Iterative Detection (BICM-ID) Using Extended Mapping in Broadband Wireless Communications with Turbo Equalization

By Dan Zhao

A thesis submitted to
School of Information Science,
Japan Advanced Institute of Science and Technology,
in partial fulfillment of the requirements
for the degree of
Master of Information Science
Graduate Program in Information Science

Written under the direction of
Professor Tadashi Matsumoto

March, 2010

Irregular Repetition Code-Based Bit-Interleaved Coded Modulation with Iterative Detection (BICM-ID) Using Extended Mapping in Broadband Wireless Communications with Turbo Equalization

By Dan Zhao (810201)

A thesis submitted to
School of Information Science,
Japan Advanced Institute of Science and Technology,
in partial fulfillment of the requirements
for the degree of
Master of Information Science
Graduate Program in Information Science

Written under the direction of
Professor Tadashi Matsumoto

and approved by
Professor Tadashi Matsumoto
Professor Yasushi Hibino
Associate Professor Isao Tokuda

February, 2010 (Submitted)

I certify that I have prepared this Master's Thesis by myself without any inadmissible outside help.

Dan Zhao
JAIST, Feb.9^{th}, 2010

Author: _____

Date: _____

Supervisor: _____

Acknowledgments

Since on April 2008 I came to Japan and started my research work under Prof. Tad Matsumoto's supervision, my life and attitude towards the scientific development has been deeply touched by Prof. Matsumoto's great enthusiasm and encouragement. This work can be successfully conducted in such a short time, which largely depends on his invaluable guidance and support. I want to forward my deepest appreciations to this incredibly kind and charming person. I am also grateful to all my colleagues in Matsumoto lab, for their friendship and help. The financial support provided by Hitachi Kokusai Electric Inc. is highly acknowledged.

My warmest thanks go to my parents X. L. Bao and H. B. Zhao., for their endless love, support and understanding. Finally, thank my closed friends for their care and help throughout my life.

Dan Zhao
JAIST Japan, Feb. 2010

Abstract

Performances of bit-interleaved coded modulation with iterative detection (BICM-ID) systems strongly depend on the matching between mapping rule and code structure. This thesis first examines the basic properties of different mapping schemes, and then proposes a combined use of extended mapping (EM) and simple repetition code. Even with such a simple structure, turbo cliff happens at a value range of signal-to-noise power ratio (SNR) $1 \sim 2dB$ to the Shannon limit. Based on this structure, this thesis further develops the efficient use of modulation doping and irregular degree-allocated repetition code with check nodes, so that we can flexibly change the shape of the extrinsic information transfer (EXIT) curves, thereby, to achieve better near-capacity performance. It is shown that EXIT analysis and chain simulation results exactly match each other. Furthermore, the system is extended to broadband single carrier signaling suffering from fading frequency selectivity, where frequency domain soft cancellation minimum mean square error equalization (FD SC MMSE) is used for the equalization of inter-symbol interference (ISI) caused by the fading. By using extended mapping the spread of the equalizer EXIT function due to fading variation can be made much smaller than using Gray mapping. With this statistical property of the EXIT functions, it is made possible to design the BICM-ID chain such that with the majority of the channel realizations, the turbo cliff happens. This indicatively suggests that outage-based adaptive transmission chain optimization is made possible with the proposed technique. The convergence property analyses are also presented in the thesis. Better performance can be achieved compared with the conventional techniques that require equivalent computational complexity.

Keywords: extended mapping; check node assisted irregular repetition code; modulation doping; EXIT analysis; FD SC MMSE

Contents

Achievements

Publications:

- D. Zhao, A. Dauch, and T. Matsumoto, "BICM-ID Using Extended Mapping and Repetition Code with Irregular Node Degree Allocations", IEEE VTC 2009-spring, Barcelona, April 26th-29th, 2009 (*Young Researcher Encouragement Award granted by IEEE VTS Japan*).

- D. Zhao, A. Dauch, and T. Matsumoto, "Modulation Doping for Repetition Coded BICM-ID with Irregular Degree Allocation", ITG/IEEE Workshop on Smart Antennas, Berlin, Feb. 16th-19th, 2009.

- D. Zhao, A. Dauch, and T. Matsumoto, "Irregular Repetition Coded BICM-ID with Modulation Doping for Turbo Equalization in Broadband Single Carrier Signaling", submitted to EURASIP Journal on Advances in Signal Processing-Advanced Equalization Techniques for Wireless Communications, currently under review.

- D. Zhao and T. Matsumoto, "A Simple BICM-ID Technique for Turbo Equalization", IEICE National Conference 2010-spring, Sendai, March 16th-19th, 2010, Accepted.

Presentation:

- D. Zhao, K. Anwar, and T. Matsumoto, "Irregular Repetition Coded BICM-ID with Extended Mapping and Doping", IEEE Workshop on Advanced Signal Processing for Wireless Communication Systems, Copenhagen, Feb. 12th-13th, 2009.

Invention Report:

- JAIST Invention Report Number 20020, "Signal Transmission Method" (patent application has been filed by Hitachi Kokusai).

List of Figures

List of Tables

Chapter 1

Introduction

Recently, digital communication systems have become an integral part of our daily life. The vision of being able to communicate and access data anywhere and anytime has driven the research and development of powerful communication systems forward at a remarkable speed. The technical challenge is to enable high data transmission rates with high power and bandwidth efficiencies. Furthermore, the aims in design of communication systems include manageable computational complexity and low end-to-end latency.

The theoretical limits of data transmission were derived by Shannon in his landmark paper presented in 1948 [3]. Shannon showed that information can be transmitted with an arbitrary low bit error rate (BER) as long as the data transmission rate is below the so-called channel capacity. To approach the capacity, high order modulation and powerful channel coding schemes are required. High order modulation improves the bandwidth efficiency by transmitting several bits per channel use through a signal point within a given signal constellation, when the operation point of the received signal power is large. Channel coding techniques introduce redundancy to improve the power efficiency. The redundancy is used to protect the transmitted data against channel impairments and enable the receiver to correct errors. The breakthrough towards capacity approaching channel code design is the idea of iterative decoding of concatenated codes, which is so-called turbo codes presented by Berrou, Glavieux, and Thitimajshima in 1993 [4]. The turbo decoder consists of the component decoders, between which soft extrinsic information is exchanged in an iterative fashion. The idea of iterative decoding has been extended flexibly in more general cases, referred to as the turbo principle [5], which can be applied to the receiver of a communication system with serial and parallel concatenated components.

Joint design of coding and modulation to optimize the performance of digital transmission schemes was proposed by Massey in 1974 [6], of which technical category is referred to as coded modulation. The coded modulation schemes include trellis-coded modulation (TCM) [7], multilevel codes (MLC) [8, 9] and bit-interleaved coded modulation (BICM)

[10]. BICM is a serial concatenation of a channel code, interleaver, and mapper. At the receiver, the signal is consecutively demapped, deinterleaved and decoded ("de-" indicates the inverse operation of "-"). Later, it was found that the performance can be significantly improved through iterative information change between the demapper and decoder based on the standard BICM receiver, according to the turbo principle. This system is usually referred to as BICM with iterative decoding (BICM-ID) [11]. Research topics on BICM-ID fall into the category of cross physical-and-medium access (PHY-and-MAC) layer optimization, with the aim of achieving close Shannon limit performance, which is also the goal of this thesis.

In principle, since BICM-ID is a serially concatenated system, analyzing its performances can rely on the area property [12] of the extrinsic information transfer (EXIT) [13] chart (see Chapter 3). Therefore, the transmission link design based on BICM-ID falls into the issue of matching between the demapper and decoder EXIT curves. Various efforts have been made in the seek of better matching between the two curves for minimizing the gap while still keeping the convergence tunnel open (see Chapter 3), aiming, without requiring heavy decoding complexity, at achieving lower threshold SNR and BER floor. It has been believed that a combination of Gray mapping and Turbo or low-density parity-check (LDPC) codes achieves the best performance, compared with other combinations for BICM-ID. However, Ref. [1] proposes another approach towards achieving good matching between the two curves by introducing different mapping rules, such as anti-Gray mapping, which allows the use of even simpler codes, such as convolutional codes, and with which still it is possible to achieve BER pinch-off (corresponding to the threshold SNR). Another idea that can provide us with design flexibility is extended mapping EM [2,14]. With EM the label length can be adjusted while staying on the same constellation diagram. This enables us to adjust the spectral efficiency not only by changing the rate of the channel code, but also changing the labeling length of the used mapping scheme. One of the major advantages of EM, instead of using higher order constellation diagrams, is that the system hardware can be optimized only for the one single constellation diagram. In this thesis, it is shown that the EXIT function of the demapper for EM is well matched to the very simple coding technique, irregular repetition code.

In fading channels with frequency selectivity, turbo equalization has been recognized as being one of the most efficient techniques that can remove the ISI in broadband single carrier signaling. A sub-optimal turbo equalization technique, FD SC MMSE filtering [15], can achieve asymptotically optimal performance without requiring heavy computational burden. However, if Gray mapping is used, FD SC MMSE's EXIT curves vary quite largely due to the fading variation and hence if the code parameter is fixed, BER performances vary significantly, according to the intersection point of the demapper and decoder's EXIT curves. As shown in Fig. 1.1, since the EXIT curves of the FD SC

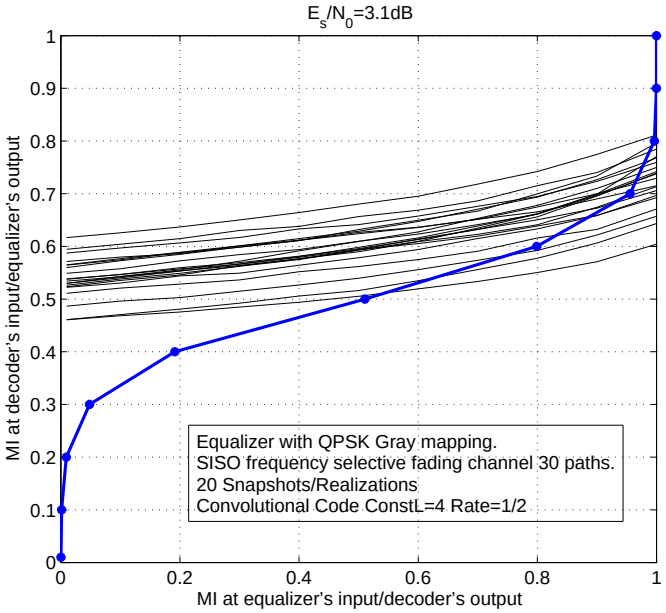

Figure 1.1: Convolutional coded FD SC MMSE equalizer with Gray mapping in SISO frequency selective fading channel with 30 paths. 20 channel realizations, and constraint length 4 rate 1/2 convolutional code. SNR=3.1dB.

MMSE equalizer spreads widely, according to the channel realizations, the intersection between them and the EXIT curve of a half rate memory 3 systematic convolutional code happens in a large range of mutual information (MI) values. This implies that sharp turbo cliff is unexpected. By using EM, the variations of EXIT curves can be compressed and therefore by combining with irregular repetition code, the variation of BER is expected to be smaller. To prove this fact is the major goal of this thesis.

The thesis is organized as follows: Chapter 2 introduces the channel and the system models assumed throughout the whole thesis. Moreover, the fundamental techniques of quadrature amplitude modulation (QAM) and the proposed code are also described in this chapter. Then, Chapter 3 investigates the EXIT chart properties as a tool to analyze and optimize iterative receivers. EXIT charts for a variety of the code parameters are presented for the proposed techniques. In Chapter 4, chain simulation results are given respectively for AWGN channel and frequency selective fading channel. Convergence outage is evaluated due to the fading variation, obtained by empirically measuring the cumulative distribution function (CDF) of BER. Performance and complexity comparisons between the proposed technique and conventional convolutional coded FD SC MMSE with Gray mapping are also conducted. Finally, the conclusions and the issues left for future study are drawn and discussed in Chapter 5.

Chapter 2

System Model

2.1 Channel Model

This thesis follows the standard conventions: the term "bit" is used to denote a binary digit, and "information bit" to denote the binary information unit. For example, a string of m bits is a sequence of symbols 0's and 1's. A random vector with m uniform independent and identically distributed (i.i.d.) components has an entropy of m information bits. Moreover, lower case symbols denote scalar quantities, boldface symbols denote vectors, underlined boldface symbols denote sequences of scalars or of vectors, and capital boldface symbols denote matrices.

Additive White Gaussian Noise (AWGN) Channel
In the AWGN channel model, the only impairment is a linear addition of wideband or white noise with a constant spectral density and a Gaussian distribution of amplitude. It produces simple and tractable mathematical model which are useful for gaining insight into the underlying behavior of a system before other phenomena are considered. The block diagram can be expressed in Fig. 2.1(A). A series of output $y(t)$ at discrete time index t is the sum of the input $x(t)$ and noise $v(t)$, where $v(t)$ is i.i.d. and drawn from a zero mean normal distribution with a variance σ_t^2. $v(t)$ is assumed to be statistically uncorrelated with the $x(t)$.

$$\begin{aligned} v &\sim \mathcal{N}(0, \sigma_t) \\ y(t) &= x(t) + v(t). \end{aligned} \tag{2.1}$$

Fading Channel
When the signal is transmitted between the base station and mobile station, because of the terrain blocking, ground clutter, multipath and so on, the receiver sees the superposition of multipath copies of the transmitted signal, each experiencing differences in attenuation,

delay and phase rotation. As the carrier frequency of a signal is varied, the amplitude and the phase of the complex baseband signal also vary. The coherence bandwidth measures the separation in frequency after which two signals will experience uncorrelated fading.

If the coherence bandwidth of the channel is larger than the bandwidth of the signal, all frequency components of the signal will experience the same fading variation. That is referred to as flat fading, for which the schematic diagram is described in Fig. 2.1(B). h is the channel gain. The received signal can be expressed as:

$$y(t) = h(t) \cdot x(t) + v(t). \tag{2.2}$$

If the coherence bandwidth of the channel is smaller than the bandwidth of the signal, different frequency components of the signal therefore experience uncorrelated fading. That scenario is referred to as frequency selective fading, as shown in Fig. 2.1(C). In this channel model, the complex channel gain vector is given by:

$$\mathbf{h} = [h(0), h(1), \cdots, h(L-1)], \tag{2.3}$$

where L is the number of paths in the frequency selective fading channel. The received signal vector $\mathbf{y} \in \mathbb{C}^{(N+L)\times 1}$ for each transmission block $\mathbf{x} \in \mathbb{C}^{N\times 1}$ can be expressed as

$$\mathbf{y} = \mathbf{H} \cdot \mathbf{x} + \mathbf{v}, \tag{2.4}$$

with $\mathbf{H} = Toepl\left([\mathbf{h}, \mathbf{0}_N]^T\right)$ and Gaussian noise vector $\mathbf{v}$, where $Toepl(\cdot)$ is the operator that makes a Toeplitz matrix from its argument vector, and N is the block length.

In this thesis, AWGN channel and frequency selective fading channel are mainly assumed. In the fading scenarios, the channel varies block by block for transmission, which is referred to as "block fading".

2.2 Bit-Interleaved Coded Modulation - Iterative Detection (BICM-ID)

The basic scheme of Bit-Interleaved Coded Modulation with Iterative Decoding with the turbo loop between the decoder and the demapper is shown in Fig. 2.2. In the iterative process, bit probabilities $P(+1)$ and $P(-1)$, or equivalently, log-likelihood ratio (LLR) defined later, updated by the decoder/demapper are fed back and used in the demapper/decoder as a priori information. To be able to achieve good performance, the outer and the inner codes that are respectively corresponding to the mapping rule and channel code have to be well designed so that the iterative information exchange

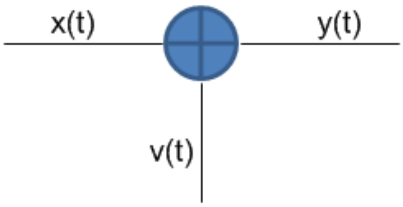

(A) AWGN Channel

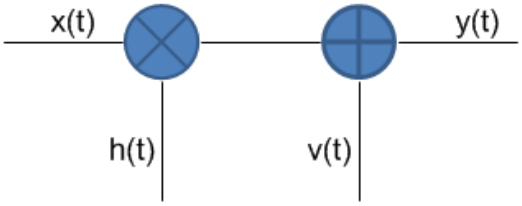

(B) Flat Fading Channel

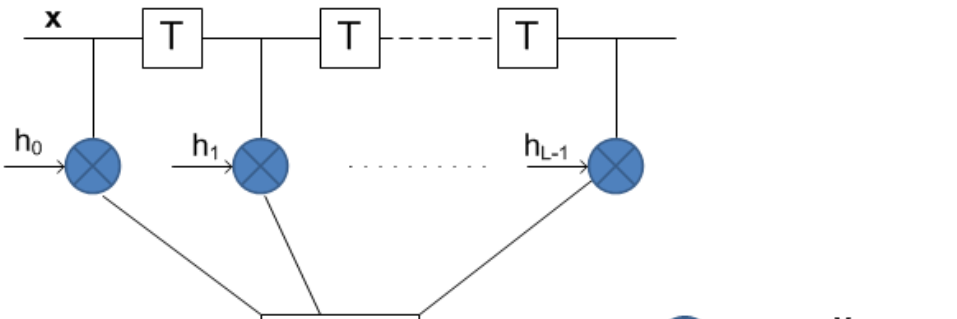

(C) Frequency Selective Fading Channel

Figure 2.1: Channel model (A) AWGN Channel, (B)Flat Fading Channel, (C)Frequency Selective Fading Channel.

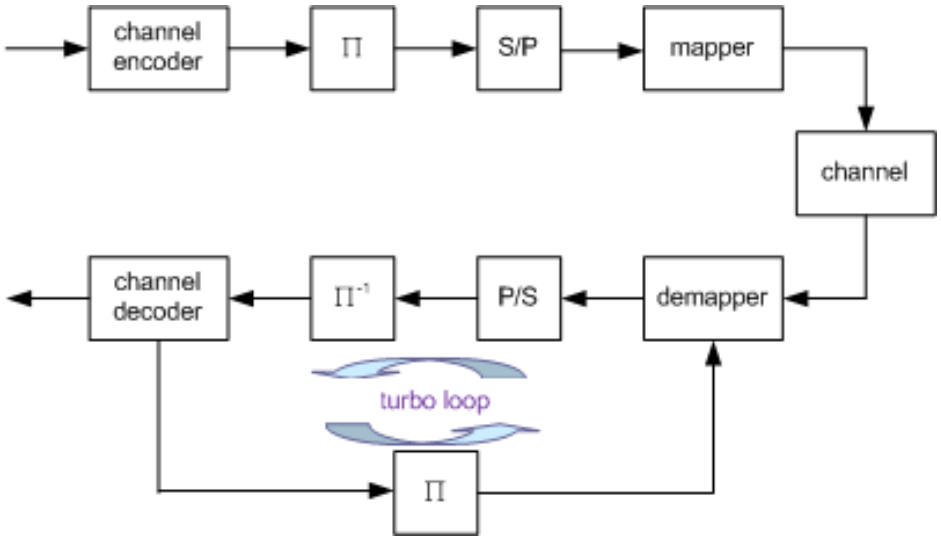

Figure 2.2: Basic scheme of BICM-ID system.

converges at a certain point. The terms, *a* priori, extrinsic and *a* posteriori information and likelihood are defined following [16].

Log-Likelihood Ratio

The log-likelihood ratio (LLR) of a binary random variable u_k is defined as

$$L\left(u_k\right) = ln\left(\frac{P\left(u_k = +1\right)}{P\left(u_k = -1\right)}\right), \tag{2.5}$$

where $P(u_k = +1)$ and $P(u_k = -1)$ are the probabilities of the information bit being 0 and 1 respectively. The LLR is also called 'soft bit', because the sign of $L(u_k)$ represents the hard decision and the magnitude $|L\left(u_k\right)|$ represents the reliability of this decision [17]. From a given LLR value it is possible to calculate the probability that $u_k = +1$ or $u_k = -1$ by using

$$\begin{aligned} P\left(u_k = +1\right) &= \frac{e^{L(u_k)}}{1 + e^{L(u_k)}} \\ P\left(u_k = -1\right) &= \frac{1}{1 + e^{L(u_k)}} \end{aligned} \tag{2.6}$$

***A* Priori Information**

The *a* priori information (L_a) is the information that expresses the amount of knowledge already known about the bit before decoding from another source. In many cases, it can be obtained from the other decoders.

Extrinsic Information

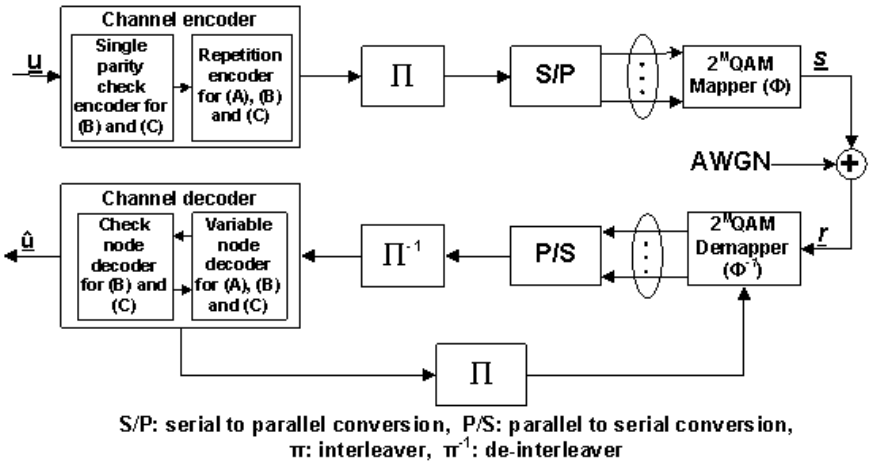

Figure 2.3: Proposed BICM-ID system scheme.

The extrinsic information (L_e) is the 'gain' of the knowledge about the bit achieved by performing decoding. It is in many cases the information about a bit calculated by a decoder using the channel reliability value, referred to as the channel LLR (L_c), and the *a* priori information provided by other decoders as input. At the output of the decoder, extrinsic information is obtained by subtracting *a* priori information from the other decoders at the output of the current decoder and also subtracting the channel value L_c. Therefore, extrinsic information depends only on the structure of the used code.

***A* Posteriori Information**

The *a* posteriori information ($L_p(u_k \mid r)$) is calculated using all available information, in the form of LLRs, of a bit. This information is calculated by the maximum *a* posteriori (MAP) algorithm which is explained in Section 2.6. By definition, the *a* posteriori LLR is expressed as:

$$L_p(u_k \mid r(t)) = L_c(t)\, r(t) + L_e(u_k) + L_a(u_k). \tag{2.7}$$

A schematic diagram of the proposed BICM-ID system is shown in Fig. 2.3. More detailed contents of each block in this system model are explained in Section 2.3-2.6.

2.3 Check Bit Assisted Irregular Repetition Code

Weak codes are not always too bad: in this thesis, we propose check bit assisted irregular repetition code for channel coding, combined with the extended mapping in the BICM-ID structure. This sub-section describes how the proposed code structure is obtained.

Repetition Code

Repetition code is the simplest coding method. Each information bit to be transmitted is

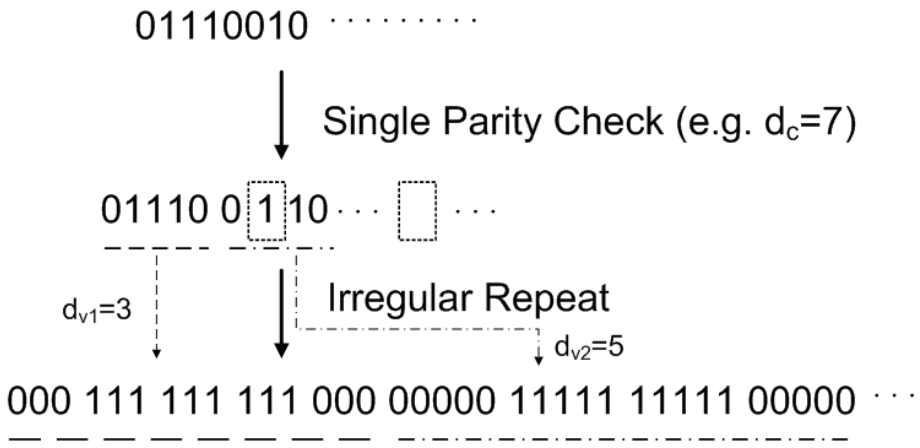

Figure 2.4: Encoding method of check bit assisted irregular repetition code.

repeated d_v times, which formulates the operation of the encoder as shown in Fig. 2.3(A). The repetition times d_v is referred to variable node degree.

Single Parity Check Code
According to single parity check rule, for every $d_c - 1$ information bits, a single parity check bit is added to the information sequence $\underline{\mathbf{u}}$, where d_c is referred to check node degree.

Check Bit Assisted Irregular Repetition Code
Information sequence $\underline{\mathbf{u}}$ is encoded by single parity check code, then followed by the encoder for repetition code. However, the repetition times d_v take different values in one whole block. Such code is referred to as having irregular degree allocations. The structure is referred to as check bit assisted irregular repetition code, as used in Fig. 2.3(C). The whole concept of this code is illustrated in Fig. 2.4.

2.4 Quadrature Amplitude Modulation (QAM)

To be able to transmit the information, the logical data in a bit sequence, has to be mapped to physical media. This process is referred to as modulation. In wireless communications, in order to convey the data, the carrier signal locates at a center frequency f_c has to change its properties according to the data format. In QAM, the carrier signal's amplitude and phase are simultaneously controlled due to the data. Note that amplitude-modulated two carriers having the same center frequency but phase-shifted by 90 degrees can be equivalently viewed as a both amplitude- and phase-modulated single carrier signal. As in many digital modulation schemes, the constellation diagram is a useful representation of the signal. With the QAM constellation, amplitudes of the both In-phase and Quadrature

components in the complex signal expression change. The assigned signal points follow the constellation diagram, and labeling patterns are determined by the mapping rule. The applied mapping rule has crucial impact on the system performance in iterative systems [18].

2.4.1 Constellation Diagram

The modulation constellation displays the signal as a two-dimensional diagram in the complex plane. Since in digital communications the data are usually binary, the number of points in the grid is usually a power of two. The widely used forms are 4QAM, 16QAM, 32QAM, and 2^M QAM where M represents bits per symbol. By moving to a higher-order constellation, it is possible to transmit more bits per symbol; however, if the mean energy of the constellation has to remain the same (for fair comparison), as

$$E\left\{\left|s\left(t\right)\right|^2\right\} = 1, \tag{2.8}$$

the constellation points must be closer together and are thus more vulnerable to noise and other impairments, which results in high BER. Therefore it can be concluded that higher-order QAM can deliver more data less reliably than lower-order QAM, given the fixed mean constellation energy.

2.4.2 Standard Mapping

For a certain constellation diagram there are M complex signal points. To each point a binary sequence, referred to as label, with length l_{map} is allocated. If $l_{map} = \log_2 M$, such mapping rule is called standard mapping as in Fig. 2.5. It is shown later that the labeling pattern plays a significant role in determining performance of BICM-ID systems. Euclidean distance spectrum was introduced in [1] to make comparison of performance between different mapping schemes. The distance spectrum is defined as the number $N_N\left(d_E, s_i\right)$ of symbols (s) in the constellation diagram (χ) $\hat{s_i} \in \chi_{\bar{b}}^p$, with the distance d_E from the symbol $s_i \in \chi_b^p$, where χ_b^p is the subset of symbols whose bit label have the value b at the p^{th} position and is its complementary subset. This distance is averaged over all bits and all M symbols. The distance spectrum without a priori information can be calculated as:

$$\bar{N}\left(d_E\right) = \frac{1}{l_{map} \cdot 2^M} \sum_{p=1}^{l_{map}} \sum_{b_p=0}^{1} \sum_{s_i \in \chi_b^p} N_N\left(d_E, s_i\right). \tag{2.9}$$

In the case with full a priori information the demapper knows all bits except the one which is to be detected by using the extrinsic information. In this case only symbol pairs

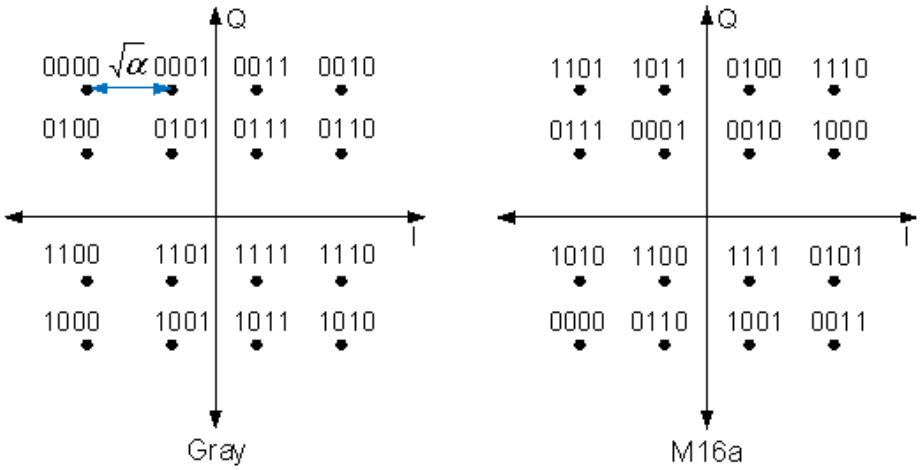

Figure 2.5: Standard mapping schemes of 16QAM

that differ in the value of just one code bit at the p^{th} position need to be considered in Eq. 2.9. For this reason the distance spectrum with and without a priori information are different. Using the distance spectrum the binary switching algorithms [19] can find the best labeling for with and without a priori information. The results of the distance spectrum from [1] are shown for the case without a priori information in table 2.1 and with a priori information in table 2.2.

d_E^2	α	2α	4α	5α	8α	9α	10α	13α	18α
Gray	0.75	1.12	1	2.25	1	0.25	0.75	0.75	0.12
MSP	1.62	1.19	0.75	2.25	0.25	0.62	0.75	0.5	0.06
M16a	1.75	1.31	1.25	1.25	0.5	0.75	0.75	0.75	0.19

Table 2.1: Distance spectrum without a priori information

d_E^2	α	2α	4α	5α	8α	9α	10α	13α	18α
Gray	0.75	0	0	0	0	0.25	0	0	0
MSP	0	0.06	0.25	0.12	0.25	0	0.12	0.12	0.06
M16a	0	0	0	0.5	0.12	0	0.12	0.25	0

Table 2.2: Distance spectrum with full a priori information

The most commonly accepted and used modulation scheme in practical systems is Gray mapping [20]. Because for BICM with no a priori information, $\bar{N}\left(d_E = shortest\right)$ dominates the performance, and Gray mapping has the smallest $\bar{N}\left(d_E = shortest\right)$ value

compared with other mapping rules; in other words, Gray mapping can carry the largest amount of information without iteration. In this case, "strong" channel codes, like turbo codes, LDPC, and convolutional codes having very large memory length, are suitable, because these codes can reach good performance even in the first iteration. With full a priori information available, however, Gray mapping should not necessarily achieve the best performance, yet non-Gray mappings would achieve better performance. For example, as shown in Table 2.2, MSP (Modified Set Partitioning) [21] and M16a mapping rules achieve $\bar{N}\left(d_E = \sqrt{\alpha}\right) = 0$ with full a priori information. This means, with full a priori, those two mappings are more robust than the Gray mapping. Therefore, in iterative systems, there is a possibility that with "weak" channel codes, like repetition codes, a non-Gray mapping can achieve better or equivalent performance.

2.4.3 Extended Mapping

The basic idea of the extended mapping [2] is to increase the length of the labeling map for a given constellation diagram. For each labeling, the length is assumed as $l_{map} = \log_2 M + x$, where x is the number of the extended bits. Therefore, there are more than 1 labeling patterns allocated to one constellation point, which results in the ambiguity for demapping when only considering the demapper part. However, in iterative decoding systems, with a priori information, by combining a certain outer code the ambiguity can be resolved. Nevertheless, there are many possible combinations of bit patterns to be allocated to the constellation points. The design goal of an optimized extended mapping with a priori information is to maximize the Hamming distance between all the labels at each signal point, and also the Hamming distance between each of the neighboring signal points. In other words, the design rule is the same as standard mapping that is to maximize the average Euclidean distance spectrum, but with full a priori information. This thesis uses the labels assigned to the each constellation point obtained by [2], so that, with full a priori information, the mutual information (MI) between the coded bit and the demapper output LLR is maximized. Fig. 2.6 shows the optimal labeling for 4QAM with $l_{map} = 3$ and 5, with the number of extended bits 1 and 3 respectively.

When a specific constellation diagram is chosen,denoted as Ψ, the capacity of the AWGN channel is given by

$$C = H\left(x\right) - H\left(x \mid y\right), \tag{2.10}$$

where it is assumed that the element signals $x \in \Psi$ are transmitted with equal probabilities and $H\left(\cdot\right)$ is the corresponding entropy. It is obvious to see that the MI is upper bounded by the number of the constellation points in this specific diagram, no matter what kind of mapping rule is involved in. According to [7], for low SNRs, the capacity loss due to the use of a specific constellation may be very small. Binary transmission is a reasonable

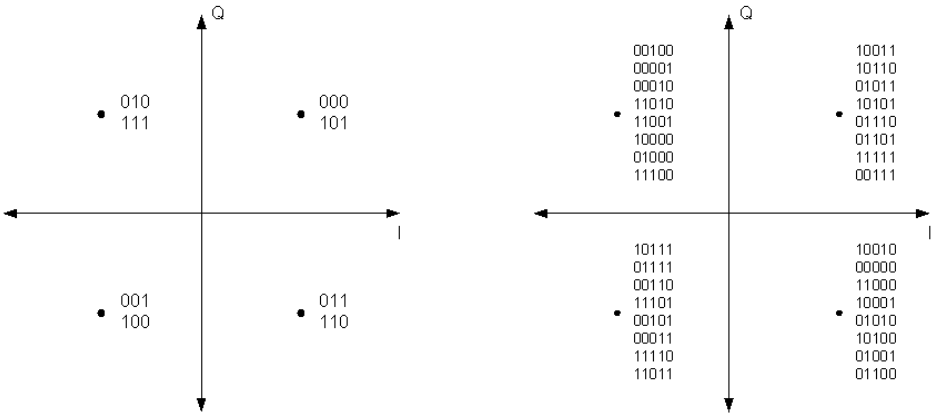

Figure 2.6: Extended mapping 4QAM $l_{map} = 3$ and $l_{map} = 5$, optimized with a priori information

proposition in small SNR range, whereas we should choose a large constellation if the channel has a large signal-to-noise ratio to achieve large spectrum efficiency.

2.4.4 Doping

When designing a new technique, in general, it is desirable that it does not require additional complexity in the transmission chain. As in ten Brink's proposed code doping techniques [22], irregular modulation [23] may satisfy this requirement where multiple different mapping schemes are used in one transmission block. One block comprised of interleaved bits with the length N is divided into P sub-blocks, each containing $\alpha_k \cdot N, k = 1...P$ bits, where $\sum_{k=1}^{P} \alpha_k = 1$ [24]. For each of the sub-blocks a different mapping scheme can be used. The label length of the used mapping scheme for the each sub block is $l_{map,k}$. The value of α_k must be chosen so that each block contains a multiple of $l_{map,k}$ coded bits. In this thesis, we use blocks comprised of two mapping schemes as shown in Fig. 2.7, where the ratio of the number of symbols mapped according to the standard mapping is defined as doping ration d. The spectrum efficiency with this scheme is given as:

$$\eta = d \cdot l_{map,1} \cdot r_c + (1 - d) \cdot l_{map,2} \cdot r_c, \tag{2.11}$$

where r_c denoted the outer code rate.

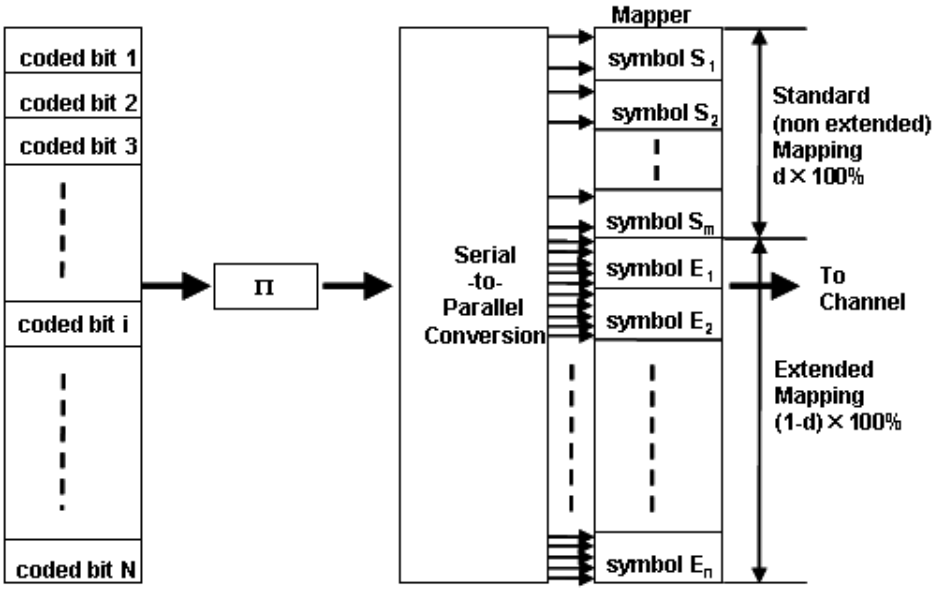

Figure 2.7: Doping block diagram.

2.5 Decoder

2.5.1 Repetition Code

Fig. 2.8(A) shows a block diagram of the repetition code decoder. The d_v bits constituting one segment, output from the de-interleaver, are connected to one variable node, where the a priori LLR to be updated is calculated by summing up the $(d_v - 1)$ LLRs, as

$$L_{e,j} = \sum_{i=1, i \neq j}^{d_v} L_{a,i}, \tag{2.12}$$

to produce the extrinsic LLR for the j^{th} bit in the segment. This process is performed for all the other bits in the same segment as well as for all the other segments independently in the frame. Finally, the updated extrinsic LLRs are interleaved, and fed back to the demapper. With the *a* priori LLRs provided in the form of the decoder's output extrinsic LLR, demapper again updates output extrinsic LLRs. This process is repeated. Obviously, the rate of this code is $1/d_v$, and the spectrum efficiency is l_{map}/d_v *bits per symbol*.

2.5.2 Repetition Code with Check Nodes

Fig. 2.8(B) shows a block diagram of the check node assisted repetition code decoder. The d_v bits constituting one segment, output from the de-interleaver, are connected to

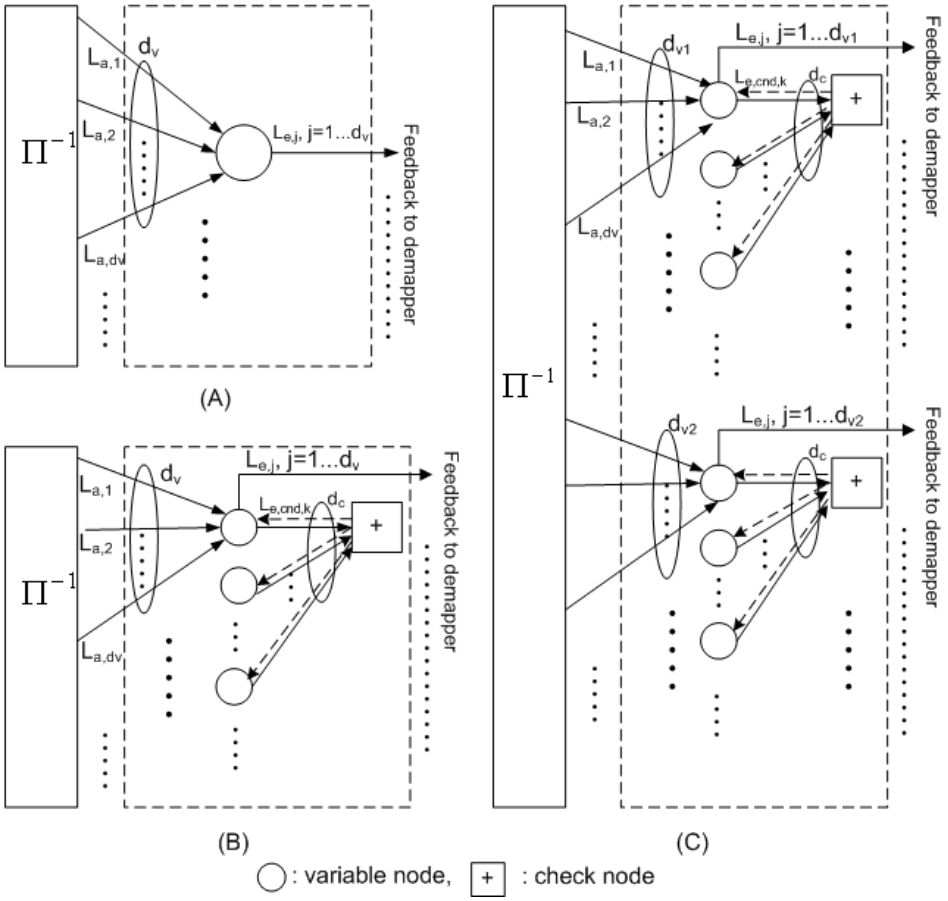

Figure 2.8: Decoder structures.

a variable node, and d_c variable nodes are further segmented and connected to a check node decoder; those demapper output bits in one segment, connected to the same variable node decoder, are not overlapping with other segments, and so is the case of the variable node segmentation. Therefore, no iterations in the decoder are required. The extrinsic LLR update for a bit at the check node is exactly the same as the check node operation in the LDPC codes, as

$$L_{e,cnd,k} = \sum_{i=1,i\neq k}^{d_c} \boxplus L_{a,cnd,i}, \tag{2.13}$$

where $\sum\boxplus$ indicates the box-plus operator [17]. The extrinsic LLR, calculated by the check node decoder, is fed back to its connected variable node decoder, where it is further combined with $(d_v - 1)$ a priori LLRs forwarded from the demapper via the de-interleaver,

as

$$L_{e,j} = L_{e,cnd,k} + \sum_{i=1, i\neq j}^{d_v} L_{a,i}. \tag{2.14}$$

This process is performed for the other bits in the same segment, and also for all the other segments independently in the same transmission block. Finally, the updated extrinsic LLRs obtained at the each variable node are interleaved, and fed back to the demapper. With the *a* priori LLRs provided in the form of decoder's output extrinsic LLR, demapper again update the demapper output extrinsic LLRs. This process is repeated. The rate of this code is $(d_c - 1)/(d_c \cdot d_v)$, and the spectrum efficiency is $l_{map} \cdot (d_c - 1)/(d_c \cdot d_v)$ bits per symbol.

2.5.3 Irregular Degree Allocations

Fig. 2.8(C) shows a block diagram of the irregular repetition code decoder. The segment-wise structure of (C) is exactly the same as that of (B), but the variable node degrees $d_{v,i}$ may have different values segment-by-segment, where i is the index of the variable node degree. The equations for the LLR update are also the same as that for (B), but the calculations have to reflect different values $d_{v,i}$ of the variable node degrees. The rate of the code is $(d_c-1)/(d_c \cdot \sum a_i \cdot d_{v,i})$, and the spectrum efficiency is $l_{map} \cdot (d_c-1)/(d_c \cdot \sum a_i \cdot d_{v,i})$ bits per symbol, where a_i represents the ratio of variable nodes having degree $d_{v,i}$ in a block.

2.6 Demapper

It is assumed that the signal is transmitted over a AWGN channel or a block frequency flat fading, and the transmission chain is properly normalized so that the received symbol energy-to-noise power spectral density ratio $E_s/N_0 = 1/\sigma_N^2$; with this normalization, we can properly delete the channel complex gain term from the mathematical expression of the channel. The discrete time description of the received signal $y(k)$ is then expressed by

$$y(k) = x(k) + n(k), \tag{2.15}$$

where, with k being the symbol timing index, $x(k)$ is the transmitted modulated signal with unit power, and $n(k)$ the zero mean complex AWGN component with variance σ_N^2 (i.e., $\left\langle |x(k)|^2 \right\rangle = 1$, $\langle n(k) \rangle = 0$, and $\left\langle |n(k)|^2 \right\rangle = \sigma_N^2$).

According to maximum *a* posteriori probability algorithm (MAP), the demapper calculates, from the received signal point $y(k)$ corrupted by AWGN, the extrinsic LLR of the

μ^{th} bit in the symbol transmitted at the k^{th} symbol timing by

$$L_e\left[b_\mu\left(k\right)\right]=\ln\frac{\sum_{s\in S_0}\exp\left\{-\frac{|y-s|^2}{\sigma_N^2}\right\}\prod_{v=1,v\neq\mu}^{l_{map}}\exp\left(-b_v\left(s\right)L_a\left(b_v\left(s\right)\right)\right)}{\sum_{s\in S_1}\exp\left\{-\frac{|y-s|^2}{\sigma_N^2}\right\}\prod_{v=1,v\neq\mu}^{l_{map}}\exp\left(-b_v\left(s\right)L_a\left(b_v\left(s\right)\right)\right)}, \tag{2.16}$$

where s denotes a signal point in the constellation, $S_0(S_1)$ indicates the set of the labels having the μ^{th} bit being 0(1), and $L_a\left(b_v\left(s\right)\right)$ the a priori LLR fed back from the decoder corresponding to the v^{th} position in the label allocated to the signal point s.

The log-MAP algorithm [25] which gives the same error performance as the MAP algorithm but is easier to implement can be used to calculate the LLRs. It uses Jacobian logarithm [26]

$$\log\left(e^{\delta_1}+e^{\delta_2}\right)=\max\left\{\delta_1,\delta_2\right\}+\log\left(1+e^{-|\delta_2-\delta_1|}\right)=\max\left\{\delta_1,\delta_2\right\}+f_c\left(|\delta_2-\delta_1|\right), \tag{2.17}$$

where $f_c\left(\cdot\right)$ is a correction function. For a finite set of real numbers $\{\delta_1,\cdots,\delta_q\}$, we can compute $\log\left(e^{\delta_1}+\cdots+e^{\delta_q}\right)$ recursively.

2.7 System Structure for Fading Channel with Frequency Selectivity

As described in Introduction, a goal of this thesis is to apply the proposed BICM-ID scheme in equalization of ISI due to frequency selectivity of the channel. Analysis and simulation results parts of this thesis are started with frequency flat block fading (AWGN) channel, because of the simplicity. If the channel exhibits frequency selectivity due to the multipath propagation, the receiver needs an equalizer to eliminate the ISI. Fig. 2.9 shows the system block diagram for frequency selective fading channel. In the following, operator $diag(\cdot)$ with a vector argument denotes a diagonal matrix with vector elements on its diagonal components. An estimate of variable is denoted by $(\hat{\cdot})$. Operator $\left(\cdot^H\right)$ denotes Hermitian (transposed complex conjugation) of the matrix, while the matrix transpose is denoted as $\left(\cdot^T\right)$. An identity matrix is denoted as $\mathbf{I}$.

Considering the frequency domain processing, all symbols are represented transmission block wise. The encoded information bits are interleaved, segmented and mapped into a block $\mathbf{x}$ having length of N symbols. Unless specified, the block indexing is omitted to simplify the presentation. Then, symbol block vector is expressed as

$$\mathbf{x}=\left[x\left(1\right),x\left(2\right),\cdots,x\left(N\right)\right]^T. \tag{2.18}$$

The channel is assumed to be static within a block, according to the block fading assump-

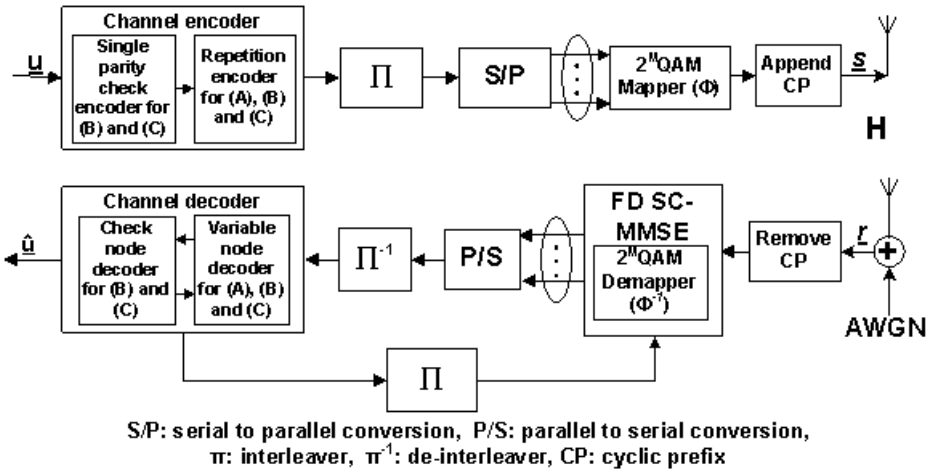

Figure 2.9: System diagram for frequency selective fading channel.

tion. With the block-wise representation, multipath propagation channel matrix $\mathbf{H}$ in Eq. 2.4 has a Toeplitz structure. In this thesis the FD SC MMSE equalization technique is assumed at the receiver, for which cyclic prefix (CP) is appended at the head of the each block so that the channel can be converted to a circulant structure, as shown:

$$\mathbf{H}^c = circ\left(\left[h\left(0\right), h\left(1\right), \cdots, h\left(L-1\right), 0, \cdots, 0\right]^T\right) \in \mathbb{C}^{N\times N}, \tag{2.19}$$

where $circ(\cdot)$ is an operator that makes circulant matrix from argument vector, and $L-1$ is channel memory length. The average channel energy is normalized to unity, i.e.

$$\sum_{i=0}^{L-1} \left\langle h\left(i\right) h\left(i\right)^* \right\rangle = 1. \tag{2.20}$$

With the circulant structure of the channel matrix $\mathbf{H}^c$, its corresponding equivalent frequency domain channel matrix becomes diagonal, as

$$\mathbf{\Xi} = \mathbf{F}\mathbf{H}^c\mathbf{F}^H, \tag{2.21}$$

where $\mathbf{F}$ is the discrete Fourier transform matrix, of which the i,j element is given by

$$\mathbf{F}_{i,j} = \frac{1}{\sqrt{N}} e^{\sqrt{-1}\cdot\frac{2\pi}{N}\cdot i\cdot j}, \quad i,j = 0,\cdots,N-1. \tag{2.22}$$

When the symbol block in (2.18) is transmitted over the frequency selective fading channel, the received signal block $\mathbf{y} \in \mathbb{C}^{N\times 1}$ can be expressed as

$$\mathbf{y} = \mathbf{H}^c\mathbf{x} + \mathbf{n}, \tag{2.23}$$

where $\mathbf{n} \in \mathbb{C}^{N\times 1}$ is a zero mean complex AWGN vector with covariance $\mathbf{E}\left\{\mathbf{n}\mathbf{n}^H\right\} = \sigma_N^2\mathbf{I}$. σ_N^2 denotes the noise variance defined by the specified SNR in decibel (dB), as

$$\sigma_N^2 = 10^{\frac{-SNR\lfloor dB\rfloor}{10}}. \tag{2.24}$$

At the receiver side, the iterative processing is invoked, where extrinsic information is exchanged between the equalizer and decoder. Since the FD SC MMSE algorithm itself is already well known, only key equations are provided in Appendix. The FD SC-MMSE equalizer calculates soft symbol vector $\mathbf{z} = [z(1), z(2), ..., z(N)]^T$ from the received sample vector $\mathbf{y} = [y(1), y(2), ..., y(N)]^T$ by the algorithm summarized in Appendix. The equalizer output is followed by demapper. By invoking the equivalent Gaussian channel approximation [Appendix Eq. (k)(l)], the extrinsic LLR of the δ^{th} bit in the soft symbol transmitted at the n^{th} symbol timing, is calculated by demapper, as

$$L_e[b_\delta(n)] = \ln\frac{\sum_{s\in S_0}\exp\left\{-\frac{|z(n)-s|^2}{\sigma_{EQ}^2}\right\}\prod_{v=1,v\neq\delta}^{l_{map}}\exp\left(-b_v(s)L_a(b_v(s))\right)}{\sum_{s\in S_1}\exp\left\{-\frac{|z(n)-s|^2}{\sigma_{EQ}^2}\right\}\prod_{v=1,v\neq\delta}^{l_{map}}\exp\left(-b_v(s)L_a(b_v(s))\right)}, \tag{2.25}$$

σ_{EQ}^2 is the equivalent noise variance at the equalizer output. With the Gaussian channel approximation, $\sigma_{EQ}^2 = \mu_{EQ}(1-\mu_{EQ})$(See Appendix for more details).

Note that with $L = 1$, the received signal suffers from only AWGN and channel gain is unity, according to Eq.(2.20). In such case, $\mathbf{z} = \mathbf{y}$, and $\sigma_{EQ}^2 = \sigma_N^2$.

Chapter 3

EXIT Chart Analysis

3.1 Basics

Extrinsic information transfer (EXIT) chart was proposed by ten Brink [13] to analyze, design, and optimize concatenated schemes with iterative processing.

The BER performance of the iterative schemes, in general, has three regions depending on SNR, as shown in Fig. 3.1. First, at low SNR, no gain over the iterations is attained and the error rate is high. The gain through information exchange between the soft-in/soft-out components is negligible. As the SNR increases, the so-called turbo cliff occurs, where the iterative system starts to converge and the error rate curve suddenly decreases. Finally, at high SNR, the error rate curve plateaus, resulting sometimes in a negligible error floor even though each receiver component has close to ideal a priori information from the other receiver components. The reason for the error floor largely depends on the type of the iterative systems, and is investigated in [25] in detail.

To analyze and optimize the convergence behavior of iterative receivers in the SNR range at the waterfall region, density evolution techniques have been proposed in [27, 28]. The main idea is to track the pdfs of the information messages exchanged in the iterative decoding algorithm. To simplify the analysis, we can assume Gaussian pdfs of LLRs [29] where a single parameter is used to describe the pdfs [30, 31]. EXIT chart [13] visualizes the density evolution of the extrinsic LLRs over the iterations using a single parameter, the average mutual information between the coded bits at the transmitter and the LLRs at the receiver. With help of EXIT charts in designing codes, asymptotic properties, including the possibility of capacity-achieving, can be visually understood, as shown in, for example, [32]. We focus on BICM-ID system, where EXIT functions of the two receiver components are the demapper and decoder.

In EXIT charts only the mutual information between the exchanged values and transmitted data needs to be tracked instead of tracking many different variables [33]. The mutual

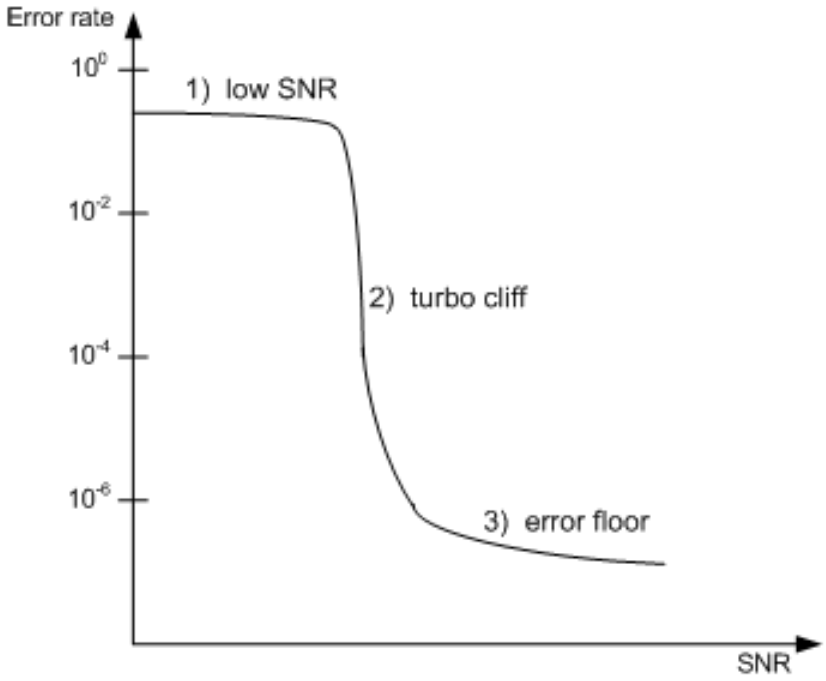

Figure 3.1: Error rate chart.

information is defined by [34]

$$I\left(x_i; y_j\right) = \sum_{i=1}^{n} \sum_{j=1}^{m} P\left(x_i, y_j\right) \cdot \log \frac{P\left(x_i, y_j\right)}{P\left(x_i\right) P\left(y_j\right)}, \tag{3.1}$$

where x_i and y_j for $i = 1...n$ and $j = 1...m$ are the two discrete random variables. This is the information content provided by the occurrence of the event y_j about the event x_i. The input of the demapper is the received signal from the channel and the extrinsic information of the channel decoder ($I_{a1} = I_{e2}$). The output of the demapper is a function of the received signal delivered by the channel and the a priori information provided by the channel decoder. In AWGN channels the output (I_{e1}) of the demapper is a function of I_{a1} and the channel 's E_b/N_0 as:

$$I_{e1} = f\left(I_{a1}, E_b/N_0\right). \tag{3.2}$$

The output of the channel decoder is a function of the demapper's output, as

$$I_{e2} = f\left(I_{a2} = I_{e1}\right). \tag{3.3}$$

In [13] the following two observations are described:

(a) For large interleavers the a priori values L_a remain fairly uncorrelated from the re-

spective channel observations over many iterations.

(b) The probability density function of the extrinsic output values L_e (are equal to the a priori input values L_a for the next decoder) approach Gaussian-like distribution with increased number of iterations.

Adopting these observations, the LLRs L can be modeled by introducing equivalent Gaussian channel, over which the known information bit x is transmitted, suffering from independent Gaussian random noise with variance σ_N^2. The AWGN equivalent channel for the log-likelihood ratio can be expressed by

$$L = \mu_L \cdot x + n_L, \tag{3.4}$$

with a mean $\mu_L = 2/\sigma_N^2$ and a Gaussian distributed n_L with variance $\sigma_L^2 = 4/\sigma_N^2$. The mean and the variance are related by:

$$\mu_L = \frac{\sigma_L^2}{2}. \tag{3.5}$$

For the EXIT chart, the MI between the coded bits B_i at the transmitter and the LLRs L_i at the receiver is used as a single parameter to characterize the pdf of the LLRs. By invoking the Ergodic property of MI, the average mutual information defined for a codeword of length N as follows [35]:

$$I = \frac{1}{N} \sum_{i=1}^{N} I\left(B_i; L_i\right). \tag{3.6}$$

Two promising approaches have been proposed to compute the mutual information for EXIT chart.

First, we can use the general equation (3.1) of the MI and simplify it using the following assumption:

$$p\left(l, b\right) = p\left(l \mid b\right) p\left(b\right); \;\; p\left(y\right) = \frac{1}{2}\left(p\left(l \mid b = 0\right) + p\left(l \mid b = 1\right)\right); \;\; p\left(b\right) = \frac{1}{2}, \tag{3.7}$$

where b and l are realizations of the random variables B of the coded bits and its corresponding LLRs, respectively. Since l has continuous values, Eq. (3.1) has to be changed to

$$I = \frac{1}{2} \cdot \sum_{b=0,1} \int_{-\infty}^{\infty} p\left(l \mid b\right) \cdot \log_2 \frac{2 \cdot p\left(l \mid b\right)}{p\left(l \mid b = 0\right) + p\left(l \mid b = 1\right)} \mathrm{d}l. \tag{3.8}$$

With this expression, MI can be conveniently computed using Monte Carlo simulation and histogram measurements.

Secondly, if we apply additional assumptions on the distributions $p(l \mid b)$, we can compute the MI as time average and avoid the numerical integration. We assume symmetric distributions $p(l \mid b=0) = p(-l \mid b=1)$, consistent distributions $p(l \mid b=0) = p(-l \mid b=1) \cdot e^l$, and therefore

$$p(l \mid b=0) = p(l \mid b=1) \cdot e^l. \tag{3.9}$$

The distributions are consistent if the LLRs are "correct", i.e. if they reflect the true reliability [28,31,36]. Often, distributions are not exactly consistent, e.g. due to suboptimal detector. However, it turns out that we can mostly assume consistency and still obtain accurate results. Combining the new constraints with equation (3.8) leads to:

$$\begin{aligned} I &= 1 - \int_{-\infty}^{\infty} p(l \mid b=0) \cdot \log_2\left(1+e^{-l}\right) \mathrm{d}l & (3.10)\\ &= 1 - E\left\{\log_2\left(1+e^{-l}\right) \mid b=0\right\}. & (3.11) \end{aligned}$$

By invoking the ergodicity, namely that the expectation can be replaced by the time average, we can approximate the MI for a large number N of samples as follows [12]:

$$I \approx 1 - \frac{1}{N}\sum_{i=1}^{N} \log_2\left(1+e^{-\tilde{b}_i \cdot l_i}\right), \ \textit{where} \ \tilde{b}_i = \begin{cases} +1, & b_i = 0 \\ -1, & b_i = 1 \end{cases}. \tag{3.12}$$

The relationship between MI and variance of LLRs can be formally described by the so-called J function [13] using the Gaussian approximation, as defined:

$$J(\sigma) = I(\sigma_L = \sigma). \tag{3.13}$$

A good emperical approximation of the J function for the binary Gaussian channel is derived in [37] as:

$$J(\sigma) = \left(1 - 2^{-H_1 \sigma^{2H_2}}\right)^{H_3} \ \textit{and} \ J^{-1}(I) = \left(-\frac{1}{H_1}\log_2\left(1 - I^{\frac{1}{H_3}}\right)\right)^{\frac{1}{2H_2}}, \tag{3.14}$$

with $H_1 = 0.3073$, $H_2 = 0.8935$ and $H_3 = 1.1064$. An application of the J function is to estimate the error rate from the EXIT chart: From the mutual information at the output of the receiver component, we compute the variance of the soft LLRs through the inverse J function as described in [38] for a serial concatenation. Assuming that the distribution $p(l \mid b)$ of the LLRs is Gaussian, the bit error rate can be easily derived from the variance

using the complementary error function, $erfc(\cdot)$, as

$$P_{BER} = \frac{1}{2} erfc\left(\frac{\sigma}{2\sqrt{2}}\right), \tag{3.15}$$

where σ^2 is variance of decoder soft output a posteriori LLR.

3.2 Area Property

We highlight one important property of the EXIT chart, namely the area theorem that relates the area under EXIT functions to the code rate and capacity. We consider the area $\mathbb{A}$ under the EXIT function $f(I)$:

$$\mathbb{A} = \int_0^1 f(I)\,\mathrm{d}I \tag{3.16}$$

For a serially concatenated scheme the following rules holds [39, 40]:

(a) The area $\mathbb{A}$ under the demapper (inner code) EXIT curve is corresponding to the constellation constrained capacity (CCC):

$$\mathbb{A} \approx C(\chi)/l_{map}. \tag{3.17}$$

(b) If the EXIT function of the a posteriori information of the outer decoder output is drawn, the area under the decoder EXIT curve is equal to the rate r_c of the code.

(c) If the demapper (inner code) and decoder (outer code) curves do not intersect, the rate of the outer code is smaller than the constellation constrained capacity and the received sequence can be iteratively decoded without any bit error. Accordingly, the area between the two curves corresponds to the rate loss.

Those relations are illustrated in Fig. 3.2.

Assuming equal SNR and the same constellation diagram, the criterion (a) is followed by: all standard mapping schemes with different arrangement of the labels have the same area under the EXIT curve[1], since the constellation constrained capacity is not dependent on the labeling rule used. This means that a high starting point with no a priori information results in a relatively low point with full a priori information and vice versa [1].

In general the designing goal is that the area under the upper curve is the same as the area under the lower curve without having those both curves intersect before reaching

[1] slightly different at low SNR range. See [2]

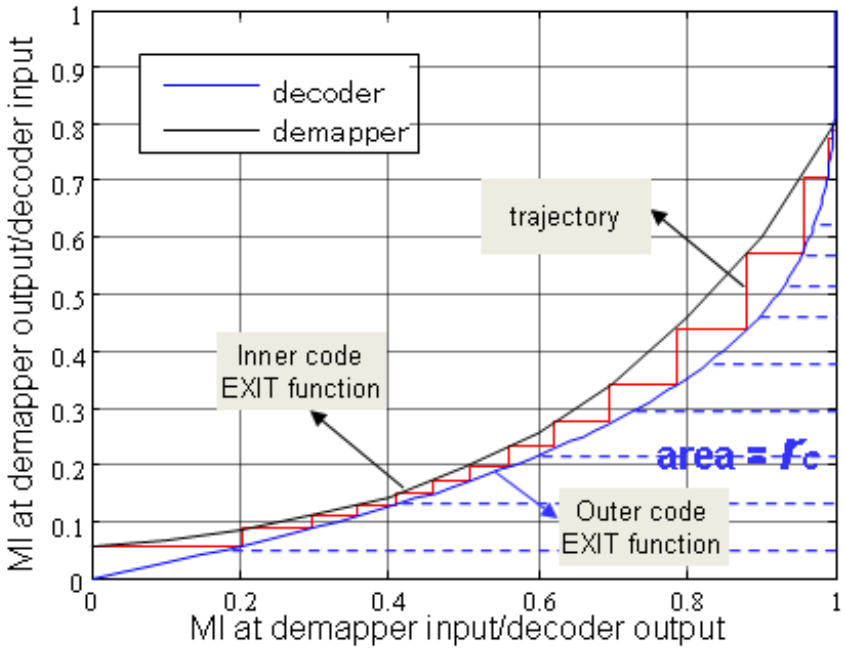

Figure 3.2: EXIT chart example of a serially concatenated system.

the ending point $I(1)$, since unless the iteration stops after the intersection [33]. In this case the rate of the code is equal to the constellation constrained capacity with the given channel conditions, and thereby no rate loss occurred .

3.3 EXIT Charts for Outer Codes

To visualize how the mutual information can be gained by the outer and the inner codes in the same EXIT chart, the x- and y-axes for the outer code are flipped, because the output of the channel decoder is the input of the demapper and vice versa.

3.3.1 EXIT Charts for Repetition Codes

The repetition code can be obtained by simply repeating the information bit d_v times. With the Gaussian assumption for the LLR distribution, the EXIT function of the repetition code is given analytically by

$$I_{e,v} = J\left(\sqrt{(d_v - 1) \cdot J^{-1}\left(I_{a,v}\right)^2}\right). \tag{3.18}$$

Where $I_{a,v}$ is the variable node input a priori MI and $I_{e,v}$ is its output extrinsic MI. $J()$ and $J^{-1}()$ are the functions that convert the square-root variance σ_L of LLR to its corresponding MI, and its inverse, respectively. Obviously, Eq. (3.18) is corresponding

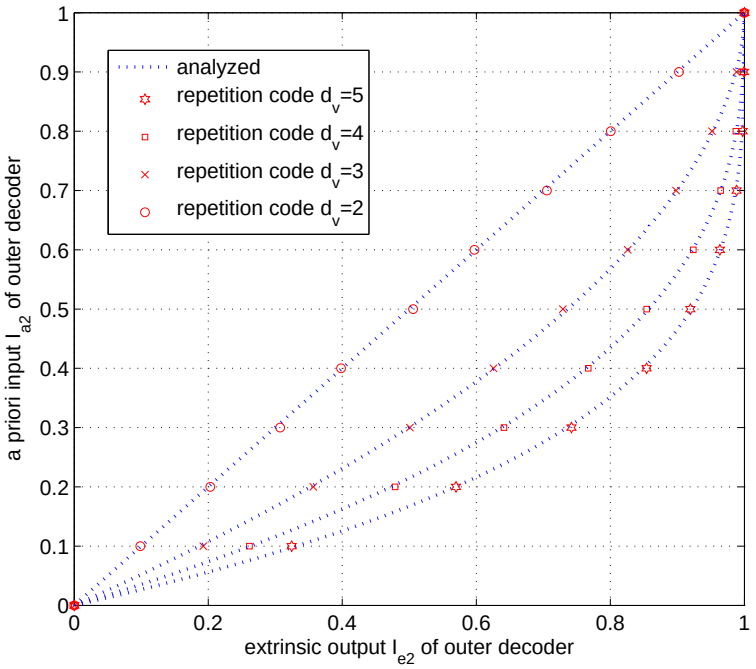

Figure 3.3: EXIT curves of repetition code with different rates, analytical calculation and simulation results.

to Eq. (2.12) for LLR update, with which $I_{a,v} = I_{e,dem}$ with $I_{e,dem}$ being the demapper output extrinsic MI. The results of the analytical calculation of Eq. (3.18) using the approximation of Eq. (3.14) in comparison to the simulation results are shown in Fig. 3.3.

3.3.2 EXIT Charts for Check Nodes Assisted Irregular Repetition Codes

Section 2.5.2 has described the decoding process of repetition code with check nodes. With the Gaussian assumption for the LLR distribution, the check node EXIT function can be analytically approximately by [25]

$$I_{e,cnd} = 1 - J\left(\sqrt{d_c - 1} \cdot J^{-1}\left(1 - I_{a,cnd}\right)\right), \tag{3.19}$$

where

$$I_{a,cnd} = J\left(\sqrt{d_v \cdot J^{-1}\left(I_{a,dec}\right)^2}\right). \tag{3.20}$$

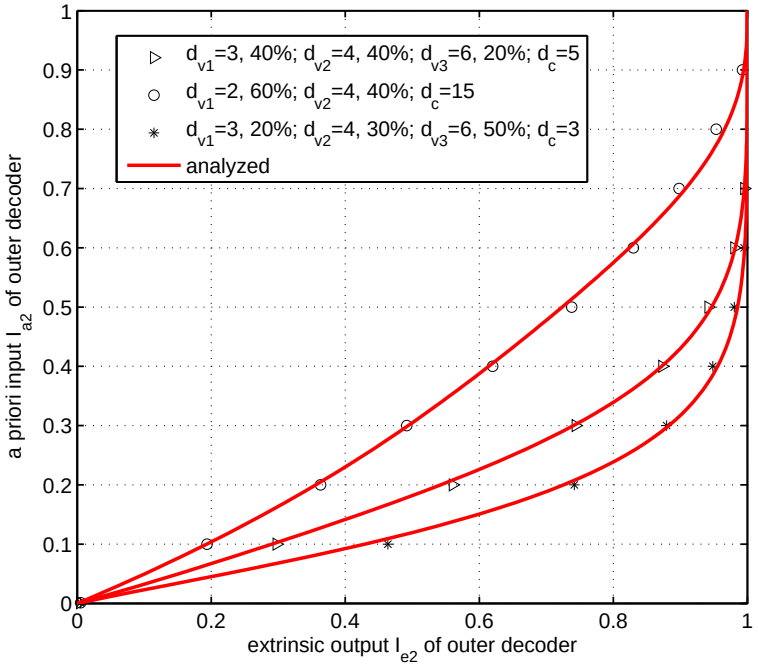

Figure 3.4: EXIT curves of irregular repetition code with different rates, analytical calculation and simulation results.

The EXIT function of the whole decoder comprised of the variable and check node decoders can be calculated by combining Eq. (3.18) and (3.19) [39], as

$$I_{e,dec} = J\left(\sqrt{(d_v - 1)\cdot J^{-1}\left(I_{a,dec}\right)^2 + J^{-1}\left(I_{e,cnd}\right)^2}\right), \tag{3.21}$$

with $I_{a,dec} = I_{e,dem}$.

For check node assisted irregular repetition code, as shown in Fig. 2.8 (C), the EXIT function of the whole decoder can be obtained by weighting the segment-wise EXIT functions given by Eq. (3.21), by corresponding to their distributions a_i, as

$$I_{e,dec} = \frac{\sum_i a_i \cdot d_{v,i} \cdot J\left(\sqrt{(d_{v,i} - 1)\cdot J^{-1}\left(I_{a,dec}\right)^2 + J^{-1}\left(I_{e,cnd}\right)^2}\right)}{\sum_i a_i \cdot d_{v,i}}. \tag{3.22}$$

Hence, the shape of the combined code EXIT function can be flexibly controlled by the irregular degree allocations. The example results of the analytical calculation of Eq. (3.22) in comparison to the simulation results are shown in Fig. 3.4. It is found that simulation results are consistent to the theoretically analyzed EXIT functions.

3.4 EXIT Charts for Inner Codes

In BICM-ID, the role of inner code is played by the mapper-demapper pair. The shape of the EXIT curve of demapper depends on the constellation diagram and the mapping rule.

3.4.1 EXIT Charts for Standard Mapping

Standard mapping can mainly be divided into Gray mapping and non-Gray mapping. With Gray mapping the slope of the EXIT curve is flat for 4QAM and almost flat for higher order QAM, while for non-Gray mapping the slope is obvious or even sharp. Because of the area property and the fact that the EXIT curves are monotonically increasing, the starting point of Gray mapping EXIT curve is higher than all other non-Gray mapping schemes, yet the ending point is the lowest. Gray mapping is optimal for "strong" codes like LDPC or Turbo Codes, but in the context of BICM-ID detection process in AWGN channels, this mapping is the worst because the iterative detection does not bring reasonable improvements. Fig. 3.5 shows the EXIT curves of 4QAM Gray and non-Gray mapping at the $SNR = 0$ and $3dB$, respectively. As SNR increases, the demapper EXIT curve of non-Gray mapping increases gradually, according to the Gaussian capacity; nevertheless, when greater than the certain value no matter how large the SNR is, the EXIT curve still cannot go beyond a certain position, because of the fact that constellation constrained capacity is almost independent of the mapping rule, and of the EXIT curve area property.

Fig. 3.6 gives three EXIT curves for different mapping rules of 16QAM. Among those, M16a and Modified Set Partitioning (MSP) mapping belong to non-Gray mapping. M16a mapping is optimized to have the highest value for the ending point $I_{a,dem}(1)$, but the lowest starting point and a sharp slope. It is optimal for "weak" codes, like the repetition codes. The MSP mapping is a compromise between the Gray and M16a mapping rules. The EXIT curve shape is a slightly concave, so that the starting and the ending points are higher than it would be connected with a straight line.

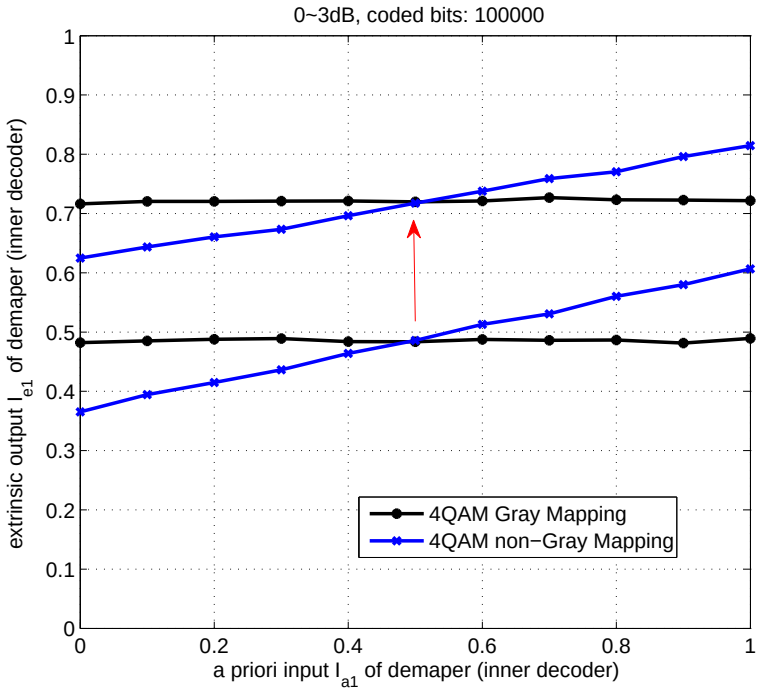

Figure 3.5: EXIT curves of 4QAM Gray and non-Gray mapping at $SNR = 0 \sim 3dB$, go up with SNR increasing.

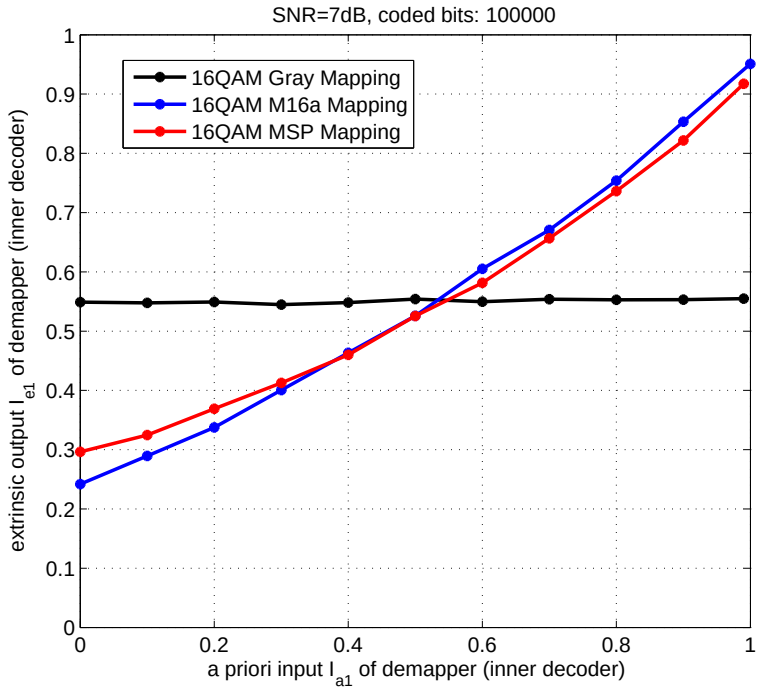

Figure 3.6: EXIT curves of 16QAM Gray, MSP and M16a at $SNR = 7dB$.

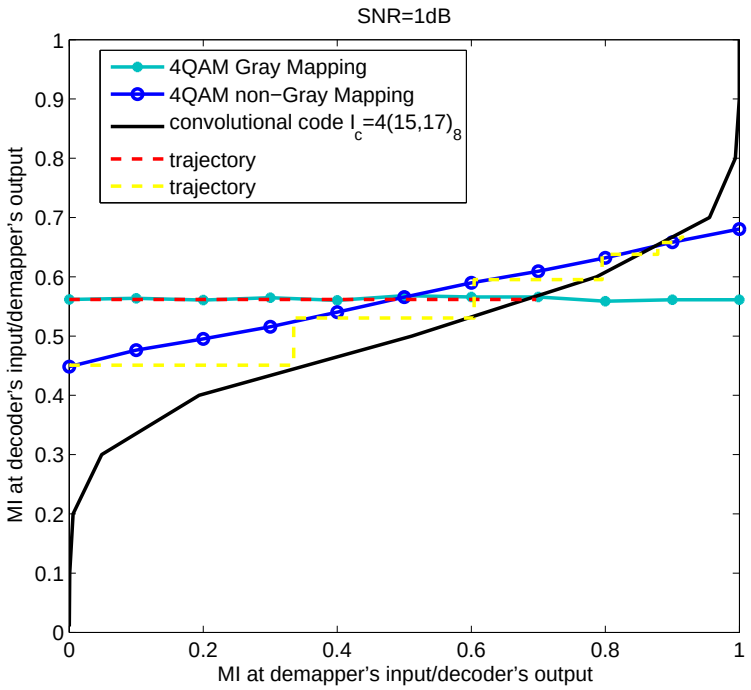

Figure 3.7: EXIT: 4QAM Gray and non-Gray mapping, with $r_c = 1/2$ convolutional code at $SNR = 1dB$.

Fig. 3.7 shows the EXIT curves of 4QAM demappers with Gray and non-Gray mapping rules together with the $r_c = 1/2$ convolutional code. After the first iteration between Gray mapping and convolutional code, these two curves get intersected, which indicates that no more extrinsic information can be achieved.

3.4.2 EXIT Charts for Extended Mapping

For extended mapping, because of the extended bits, detecting the signal is more ambiguous than the standard mapping. Therefore, the EXIT curve is significantly lower than the standard mapping, as the 4QAM example shown in Fig. 3.8. Moreover, according to Eq. (3.17), the maximum area $\mathbb{A}_{EM,max}$ under the EXIT curve of extended mapping can be calculated by

$$\mathbb{A}_{EM,max} = \frac{\log_2 M}{\log_2 M + x}, \tag{3.23}$$

even if $SNR \to \infty$, with x being the number of extended bits. The upper bounds are highlighted in the red curve in Fig. 3.9 for 4QAM extended mapping with l_{map}=3.

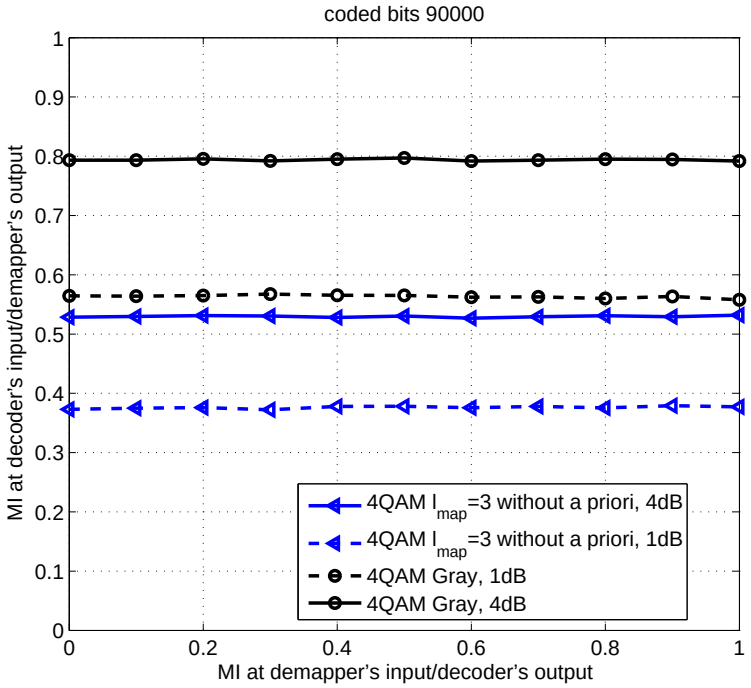

Figure 3.8: EXIT chart: 4QAM Gray mapping and EM l_{map}=3.

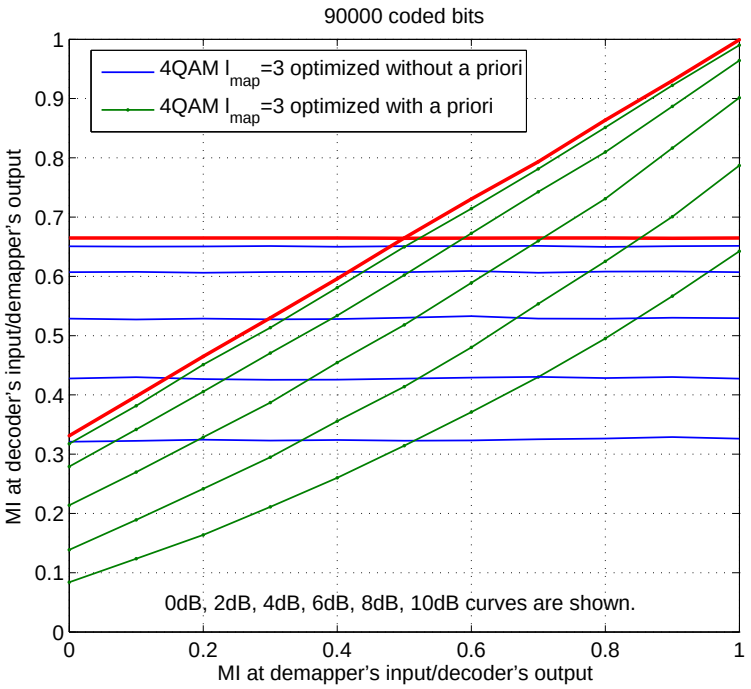

Figure 3.9: EXIT chart: 4QAM EM l_{map}=3, without a priori and with a priori, upper bounded with SNR increasing.

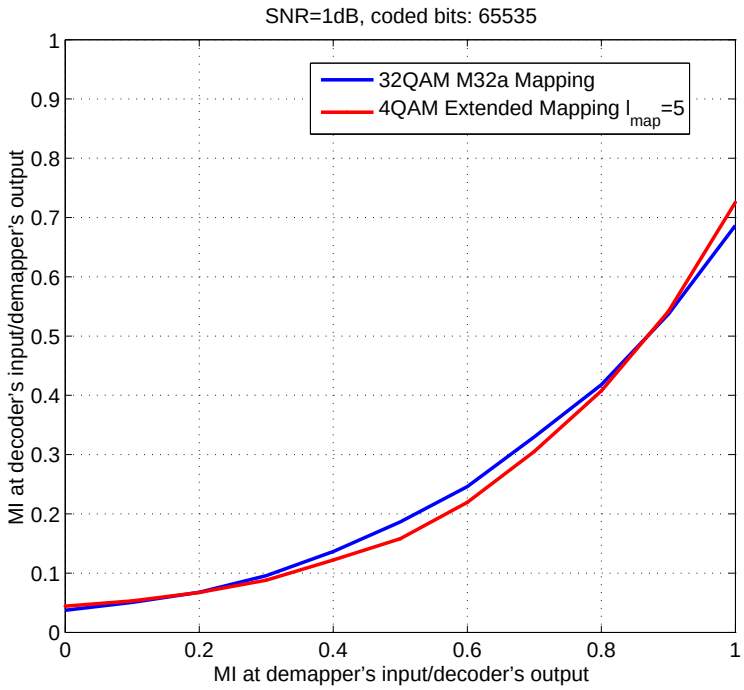

Figure 3.10: EXIT chart: 32QAM M32a and 4QAM EM l_{map}=5 at $SNR = 1dB$.

The EXIT curves of extended mapping schemes optimized without a priori information have a flat slope, similarly to Gray mapping. The flat slope indicates that the ambiguity cannot be solved even by using a priori information. On the other hand, the shape of the EXIT curve with extended mapping optimized with full a priori information has a sharper slope, as shown in Fig. 3.9.

The EXIT function for the 32QAM M32a mapping together with the 4QAM extended mapping with the label length $l_{map} = 5$ is plotted in Fig. 3.10 for comparison. Even though the both mappings have the same label length the shape of the EXIT function differs slightly. This can be explained by the fact that different constellation diagrams are used. For lower SNR values the end point for $I_{a,dem}(1)$ with extended mapping is higher than standard mapping. This can be understood by the fact that the 4QAM constellation diagram is more robust against noise than a higher order constellation diagram and by using a priori information the ambiguity can be resolved.

3.4.3 EXIT Charts for Modulation Doping

By modulation doping, a very flexible adaption of the demapper EXIT curve can be achieved. Fig. 3.11 shows EXIT curves with doped modulation using two different constellation diagrams, and Fig. 3.12 shows that using the 4QAM constellation diagram with

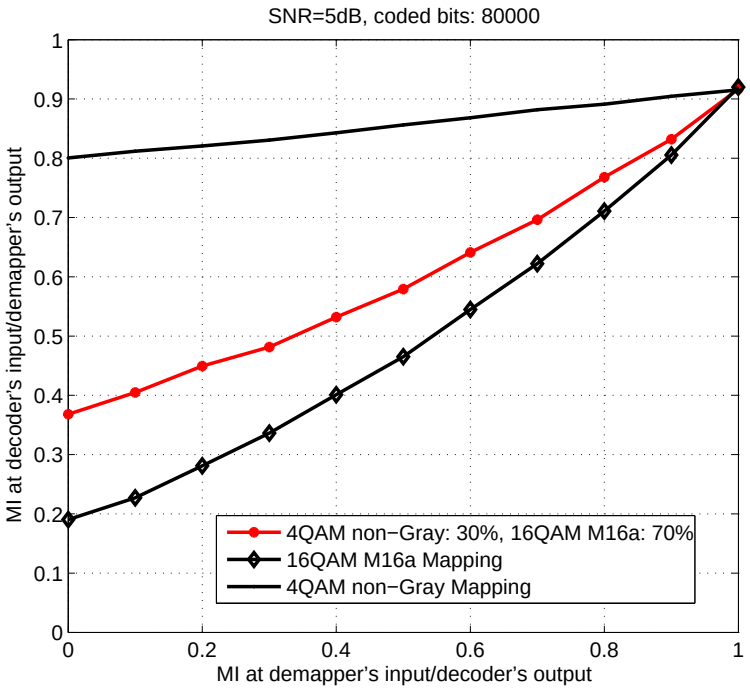

Figure 3.11: EXIT chart: modulation doping using 4QAM non-Gray: 30% and 16QAM M16a: 70% at $SNR = 5dB$.

two different label lengths $l_{map} = 2$ and $l_{map} = 5$. In the latter case, the rate can be adapted to the actual channel conditions, while staying on the same constellation diagram.

The EXIT function with modulation doping can be calculated by a linear combination of the EXIT functions of each component mapping rule [23]:

$$I_{e,dop} = \sum_{k=1}^{P} I_{e,k}, \tag{3.24}$$

where P is the number of component mapping rules, and $I_{e,k}$ is the mutual information at the k^{th} demapper output.

The EXIT curves using different doping ratios with two different 4QAM mapping label lengths were evaluated through simulations, and the results shown in Fig. 3.12. It is found that a flexible adaption is possible by changing the doping ratio. The advantage of doping with EM combined with the standard mapping is that the EM can be used for lower SNR values because the maximum starting point ($I_a(0)$) of the EXIT curve can be lifted up by the doped standard mapping. Moreover, only extending the label length of some of the mapped symbols, yet without switching the constellation diagram, it is made feasible

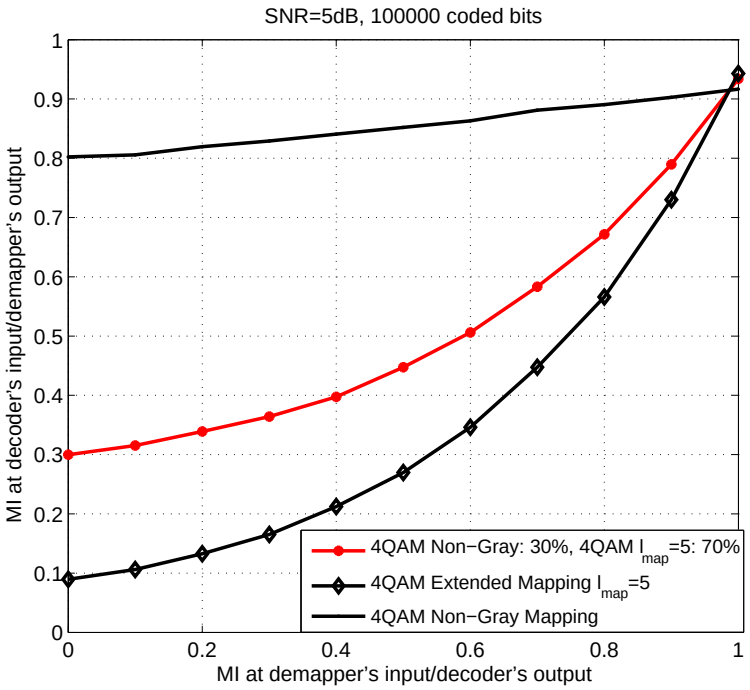

Figure 3.12: EXIT chart: modulation doping using 4QAM non-Gray: 30% and 4QAM $l_{map} = 5$: 70% at $SNR = 5dB$.

and tractable to adapt the system to the channel conditions.

3.5 EXIT Charts for Turbo Equalizer

The whole equalizer's convergence property can be represented by combining the demapper and equalizer's EXIT functions. As noted above, with extended mapping the left most point of the demapper EXIT curve is significantly low compared with Gray mapping. The MMSE equalizer further decreases the left most point of the equalizer EXIT function due to noise enhancement [41]. So the EXIT curve of the equalizer has a larger slope decay than the curve depending only on the demapper. However, because of non-negativity of the mutual information, its variation in the presence of fading has to be smaller than with Gray mapping. Fig. 3.13 shows examples of the equalizer-demapper combined EXIT functions in various fading realizations where 30 path frequency selective fading was assumed. It is found by comparing Figs. 1.1 and 3.13, that the EXIT variation with extended mapping is much smaller than with Gray mapping. This invokes the idea that even without changing the parameters of the code such as node degrees and their distributions frame by frame, BER performance can be made less sensitive to the fading variation.

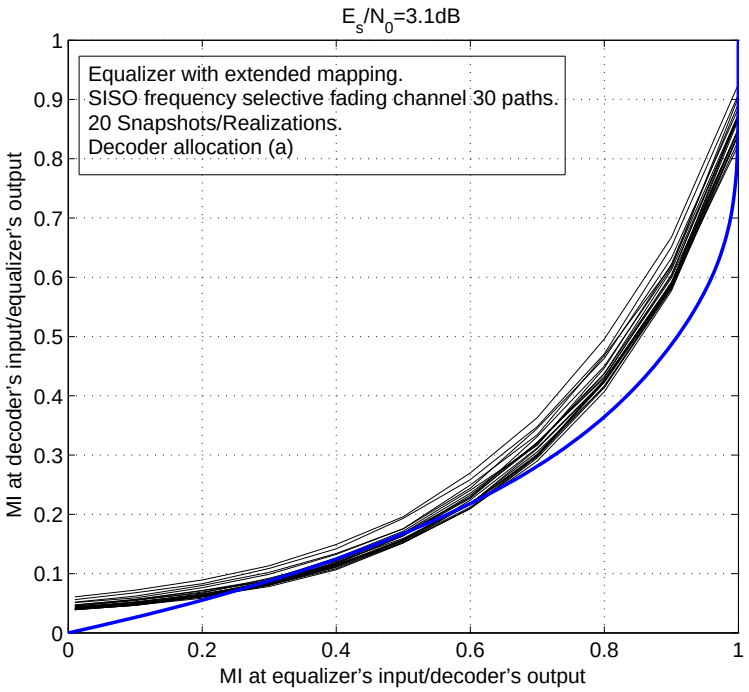

Figure 3.13: EXIT chart: FD SC MMSE equalizer with 4QAM $l_{map} = 5$ and convolutional code with constraint length 4 rate 1/2 at $SNR = 3.1dB$.

Chapter 4

Simulation Results

Given the observations of the transmission chain described in the previous sections, to achieve lower threshold SNR yielding BER pinch off as well as BER floor in BICM-ID system, besides the conventional technique which is Gray mapping combined with Turbo or LDPC codes, other approaches are now found to be within the expectation. As Fig. 4.1 shows, the EXIT chart of 16QAM M16a mapping combined with convolutional codes with constraint length l_c of 4 and repetition code d_v=3. While for the convolutional code with $l_c = 4$ both EXIT curves intersects at a low value range of mutual information, for repetition code $d_v = 3$ no intersection occurs. In this case, non Gray mapping is applied, where the EXIT curve has a sharp decay, and well matched to the weak code (=repetition code). Extended mapping, as analyzed in the last chapter, also hold the similar shape of EXIT curves, moreover, it can stay in the lower constellation diagrams. Furthermore repetition code is the weakest and simplest code among all error correction codes. The encoding and decoding operations require very low complexity and thereby, proposing this new jointly optimization method for modulation and coding technique in BICM-ID is highly motivated. In Section 4.1 chain simulations are performed in AWGN channel mode. Furthermore, to see the impact of compressing the variation of the equalizer-demapper combined EXIT function in frequency selective fading channels, chain simulation results with these techniques are also demonstrated in Section 4.2, and compared with the conventional convolutional coded Gray mapping with the respect of computation complexity.

4.1 AWGN Channel

4.1.1 Standard/Extended Mapping with Repetition Code

Standard Mapping with Repetition Code

For standard mapping schemes, increasing the labeling length, in other words, increasing

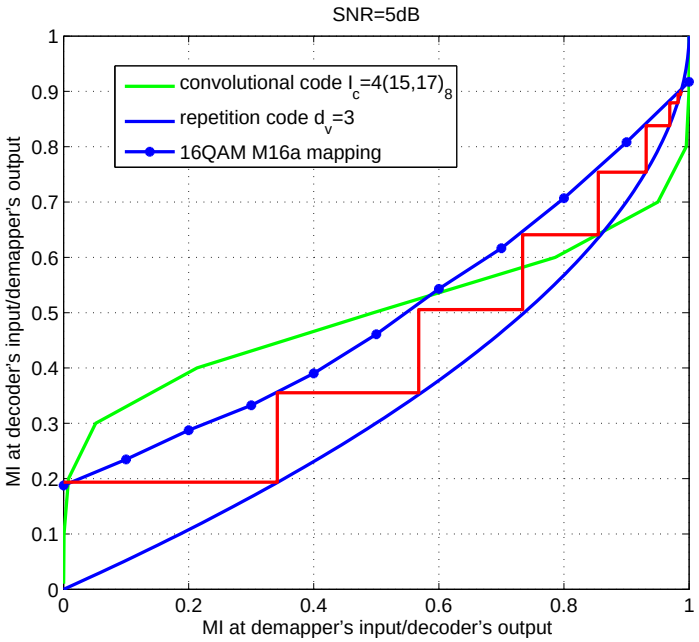

Figure 4.1: EXIT chart: 16QAM M16a combined with convolutional code $l_c = 4$.

the order of constellation diagram, enables the use of low rate repetition codes while keeping the spectrum efficiency constant. Furthermore, the use of the mapping rule optimized with full a priori information with long labeling length lifts up the EXIT end point $I_a(1)$ and pushes down the value $I_a(0)$. Nevertheless, using a higher order constellation diagram causes additional complexity at the transmitter as well as the receiver. Fig. 4.2 compares 4QAM non-Gray, 16QAM M16a and 32QAM M32a mapping schemes with several sizes of constellation diagrams and labeling lengths, with different rates $r_c = 1/d_v$ of repetition codes respectively, aiming to keep the spectrum efficiency constant as $r = r_c \cdot l_{map} = 1$ bit/symbol. The circles in the figure indicate the intersection points between the demapper and decoder EXIT curves. Among those three combinations, it is observed that the intersection of 32QAM M32a and $d_v = 5$ repetition code case happens at the highest value of mutual information, which results in the lowest BER. Despite of the fact that the intersection point is quite close to $I_a(1)$, it is still not exactly $I_a(1)$, therefore it should result in the BER floor.

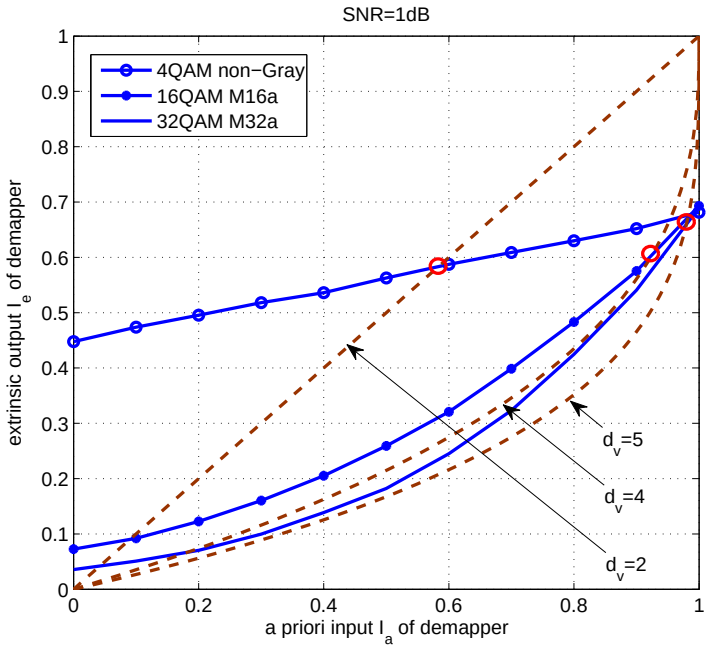

Figure 4.2: EXIT chart: 4QAM, 16QAM, 32QAM combined with different repetition codes with $d_v = 2, 4, 5$.

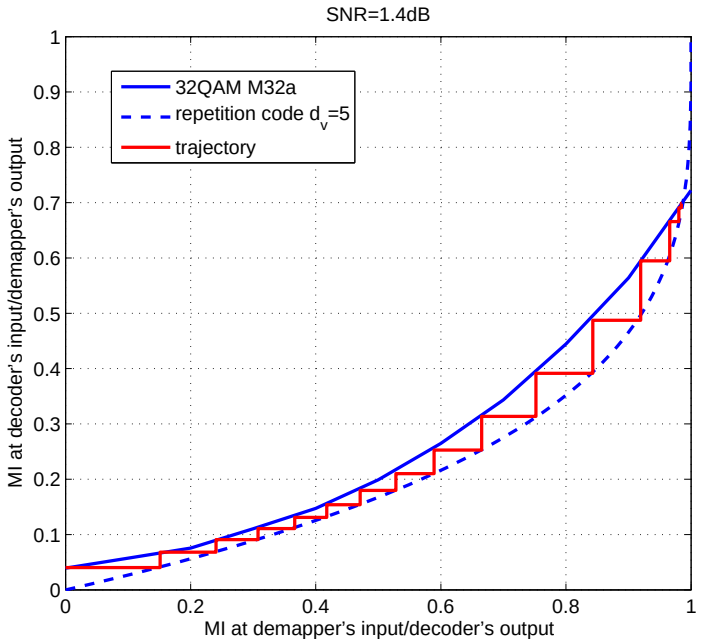

Figure 4.3: EXIT chart: 32QAM M32a combined with repetition code $d_v = 5$ at $SNR = 1.4dB$.

In the chain simulation, 32QAM M32a mapping combined with the $r_c = 1/5$ repetition code is used. The EXIT curves in Fig. 4.3 are very close to each other. The rate loss represented by the gap between the two curves is minimized due to the design rule described in section 3.2. The trajectory within the EXIT chart indicates that the iterative detection is successfully performed, yielding the final intersection point reached.

Extended Mapping with Repetition Code

With high order modulation in a low SNR value range, achieving a spectrum efficiency of one bit per channel use is impractical due to the additional complexity, such as hardware implementation and signal impairment. Extended mapping avoids the necessity of using high order constellation diagrams. Furthermore, with extended mapping the adjustment to the channel condition can be performed by changing the labeling length instead of changing the constellation diagram; even though one single constellation diagram cannot be always used over the entire SNR value range because of the saturation of the EXIT curve at high SNR values; in other words, because constellation constrained capacity as described in Section 3.2 is depending on the SNR. Using this technique, it is made possible to reduce the system complexity by using single fixed constellation diagram best matched to the combination of a repetition code and a labeling length, given a channel condition. This enables the transmitter and receiver to be optimized for a certain constellation diagram, according to practical limitations such as limited dynamic range and linearity of the amplifiers. Fig. 4.4 shows the EXIT curves of 4QAM extended mapping with a couple of labeling lengths and repetition codes with different rates. An important observation is that the EXIT curves are similar to the standard mapping shown in Fig. 4.2. Fig. 4.5 shows the EXIT chart for 4QAM extended mapping $l_{map} = 5$ optimized with full a priori information and a rate $r_c = 1/5$ repetition code. At $SNR = 1.4dB$ the tunnel between the demapper and the decoder EXIT curves suddenly opens, so that the trajectory is able to sneak through the tinny tunnel to finally approach the intersection point.

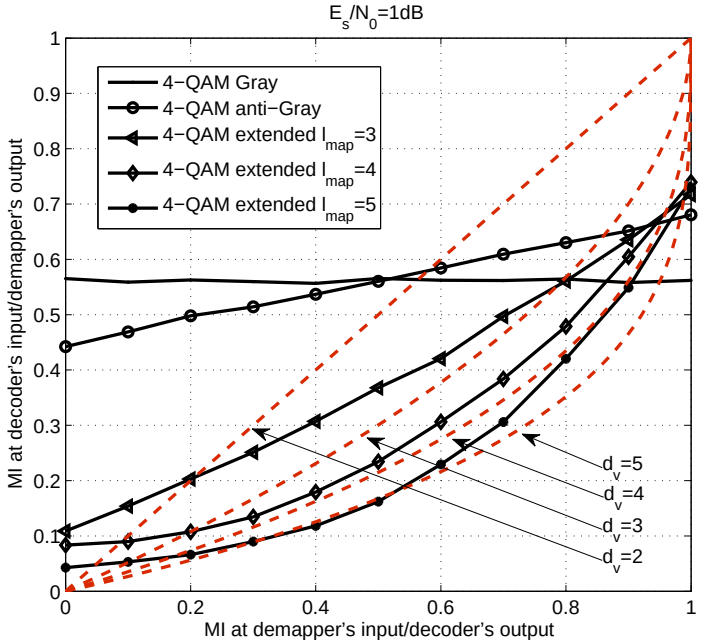

Figure 4.4: EXIT chart: 4QAM extended mapping with $l_{map} = 2 \cdots 5$ combined with different repetition codes with $d_v = 2 \cdots 5$.

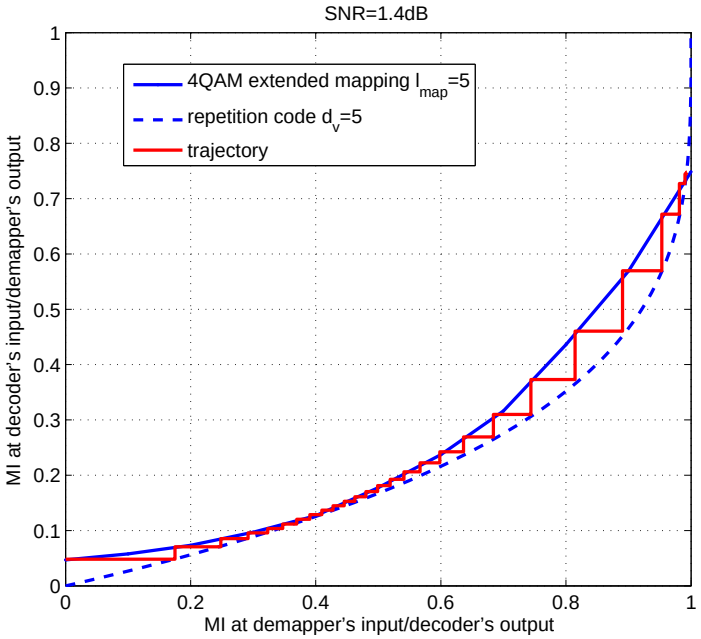

Figure 4.5: EXIT chart: 4QAM extended mapping $l_{map} = 5$ combined with repetition code with $d_v = 5$.

The BER performances of extended mapping 4QAM and 32QAM M32a mapping both combined with repetition code are shown in Fig. 4.6, while keeping the system spectrum efficiency at 1 bit/symbol. It is found that the BER of $l_{map} = 3$ EM 4QAM with $d_v = 3$ repetition code only slowly decreases as SNR increases; nevertheless, with $l_{map} = 5$ EM 4QAM with $d_v = 5$ repetition code, the turbo cliff happens at $SNR = 1.4dB$. Moreover, with 32QAM M32a mapping, a turbo cliff happens at $SNR = 0.9dB$, which is $0.5dB$ different from with $l_{map} = 5$ EM 4QAM's case. However, it should be emphasized that modulation and demodulation hardware for those two mapping rules are quite different. Therefore, the $0.5dB$ loss in SNR at the turbo-cliff point can well be compensated by the hardware complexity reduction.

4.1.2 Extended Mapping with Irregular Repetition Code

With the technique shown in Section 4.1.1, the adjustable parameters are only l_{map} and d_v, which indicates that BER cliff cannot be flexibly achieved at different SNR values and BER floor is relatively high. As Fig. 4.7 shows, at $SNR = 3.1dB$, after introducing the check node to repetition code, the right part of decoder EXIT curve is further pushed to the right hand side so that the intersection point is closer to $I_a(1)$, which results in the lower BER floor. However, the large gap between the demapper and the decoder EXIT curves still exists. By using irregular repetition code, better curve fitting is made possible by carefully choosing the degree allocations as given in Fig. 4.7(C). The trajectory from the chain simulation is exactly matched to the theoretically analyzed EXIT curves. Two BER curves with $l_{map} = 5$ EM 4QAM with irregular repetition code are shown in Fig. 4.8, together with $l_{map} = 5$ EM 4QAM and $d_v = 5$ repetition code to demonstrate the design flexibility. The trade-off between SNR threshold, BER floor and the code rate can be controlled flexibly by utilizing the degrees-of-freedom in choosing the code parameters.

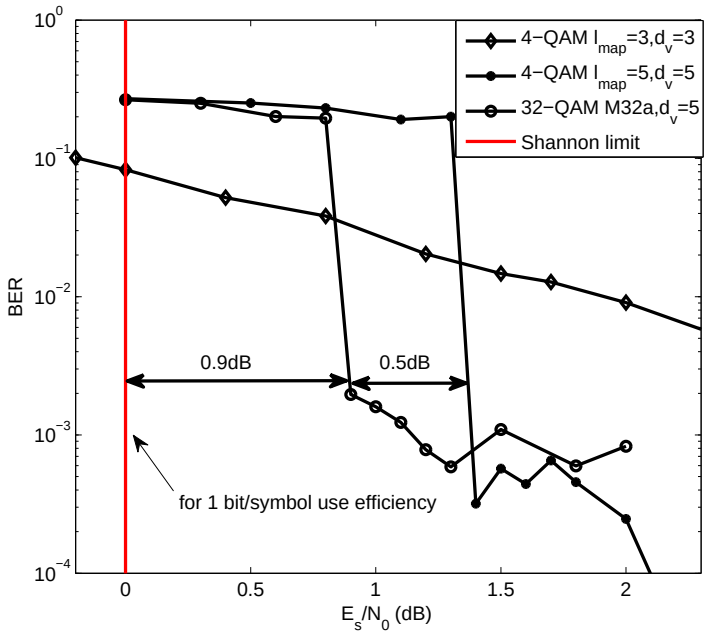

Figure 4.6: BER chart: 4QAM EM $l_{map} = 3, 5$ combined with repetition codes with $d_v = 3, 5$ and 32QAM M32a combined with repetition code with $d_v = 5$.

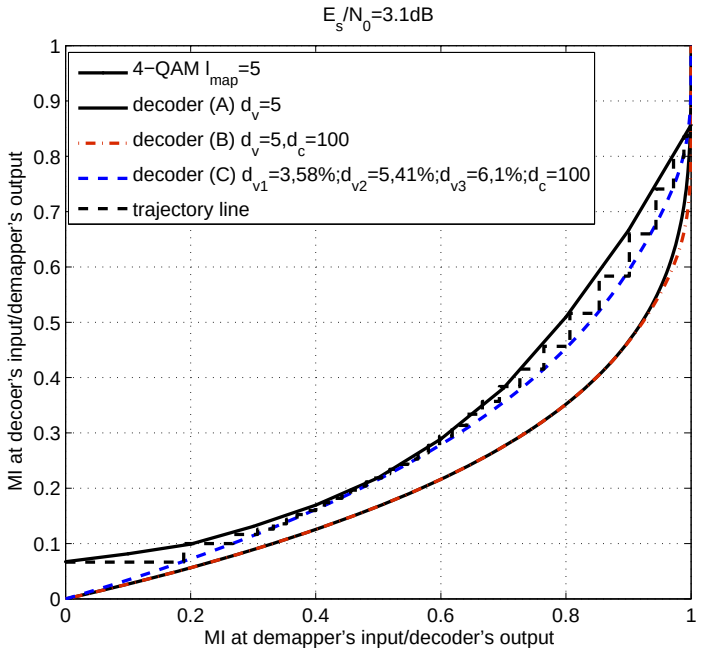

Figure 4.7: EXIT chart: 4QAM EM $l_{map} = 5$ combined with 3 kinds of repetition code due to structures (A), (B) and (C).

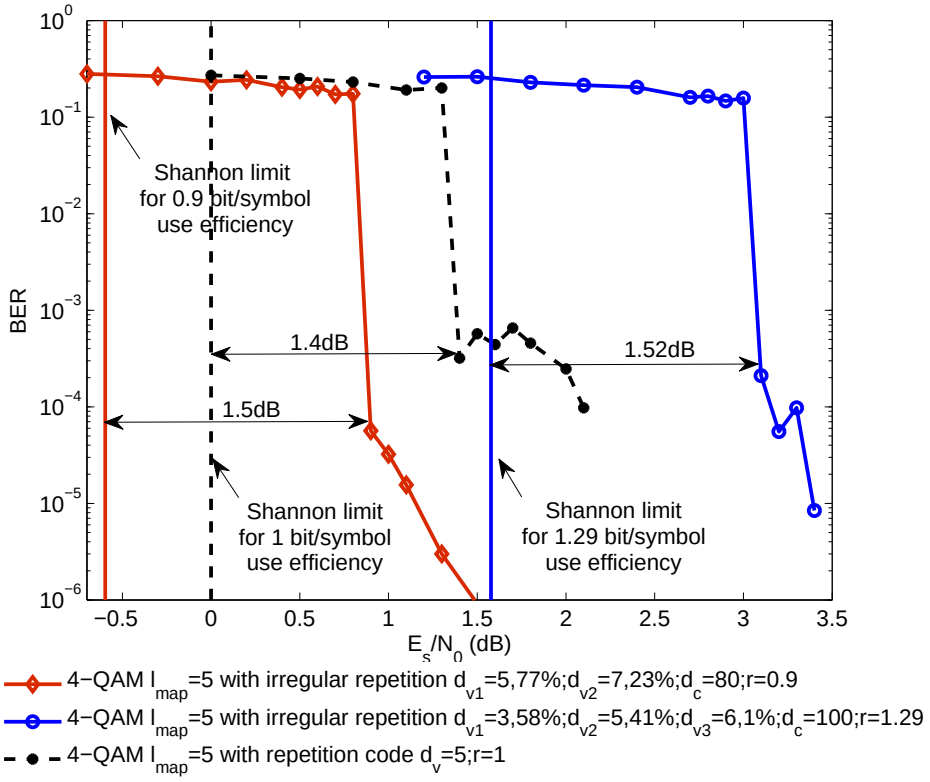

Figure 4.8: BER curves optimized by irregular repetition code.

4.1.3 Capacity Achieving

The observations above indicate that with the design flexibility made available by introducing the irregular structure, we can flexibly control the threshold SNR and the error floor, and thereby achieve near capacity performance. Nevertheless, as noted in Section 2.4.3 and 3.2, extended mapping does not increase constellation constrained capacity when using the same constellation diagram. Therefore, to achieve near Gaussian capacity at a SNR value range where the Gaussian capacity is larger than constellation constrained capacity, obviously we should move to higher order modulation. Fig. 4.9 shows the spectrum efficiency represented in bits per symbol achieved by the proposed technique versus threshold SNR for $l_{map} = 5$ 4QAM and $l_{map} = 6$ 16QAM with various irregular degree allocation parameters, which are summarized in Table 4.1. For 16QAM the optimal drawn from [2]labeling pattern is shown in Appendix.

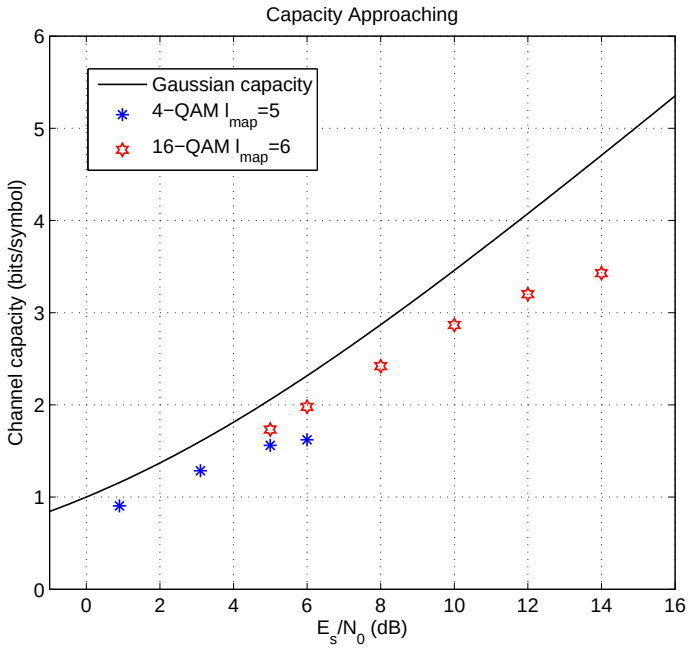

Figure 4.9: Capacity approaching with 4QAM $l_{map} = 5$ and 16QAM $l_{map} = 6$.

	$E_s/N_0(dB)$	d_{v1}, a_1	d_{v2}, a_2	d_{v3}, a_3	d_c	bits/symbol
4QAM$l_{map} = 5$	0.9	5, 0.77	7, 0.23		80	0.9043
	3.1	3, 0.58	5, 0.41	6, 0.01	100	1.2857
	5	2, 0.45	4, 0.53	6, 0.02	50	1.5605
	6	2, 0.68	5, 0.32		25	1.6216
16QAM$l_{map} = 6$	5	3, 0.65	4, 0.25	5, 0.1	260	1.7324
	6	2, 0.1	3, 0.78	4, 0.12	280	1.9797
	8	1, 0.44	2, 0.26	3, 0.3	4	2.4197
	10	1, 0.43	2, 0.57		4	2.8662
	12	1, 0.5	2, 0.5		5	3.2000
	14	1, 0.6	2, 0.4		5	3.4286

Table 4.1: Degree allocations of the codes shown in Fig. 4.9

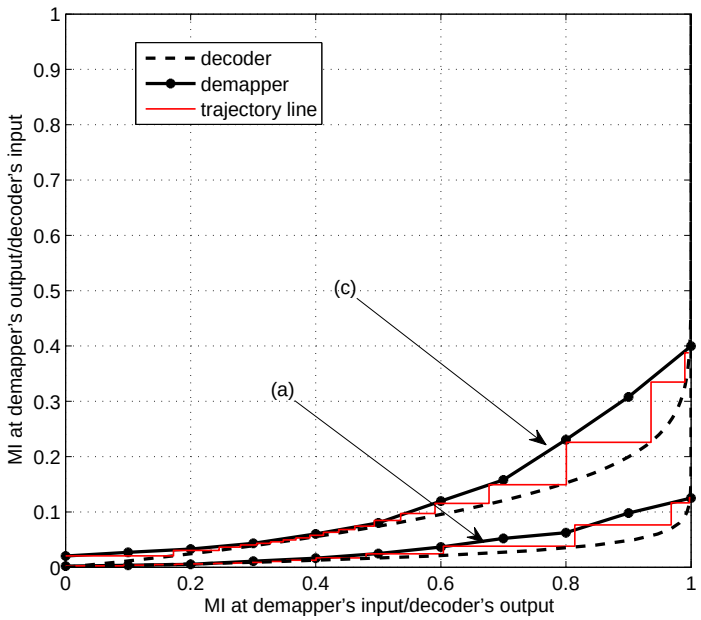

Figure 4.10: EXIT chart: Low rate design cases using modulation doping and irregular repetition code.

4.1.4 Doping with Irregular Repetition Code (Low Rate Code)

With very low SNR, the left part of extended mapping EXIT curve is too low to leave enough space for the matched decoder EXIT curves. So it is not suitable in designing BICM-ID with very low rate codes that achieve the BER pinch-off at very low SNR. To solve this problem, this thesis applies the idea of modulation doping to lift up the left most part of the demapper EXIT curves, and the amount of lifting-up depends on the doping ratio. Fig.4.10 shows EXIT curves of some representative design examples using $l_{map} = 5$ extended mapping 4QAM doped by standard mapping 4QAM: their corresponding code design parameters and SNR threshold values are summarized in Table 4.2. A series of chain simulations for the code designs shown in Table 4.2 has been conducted to verify the advantageous characteristics of the techniques proposed. The results of the chain simulations conducted to draw the trajectories for the code parameters shown in Table 4.2 are also shown in Fig. 4.10. It should be emphasized that the trajectory and EXIT curve are exactly consistent to each other. Fig. 4.11 shows the BER performance for the code design of Table 4.2. It is observed that the BER pinch-off happens exactly at the values indicated by the EXIT chart analysis.

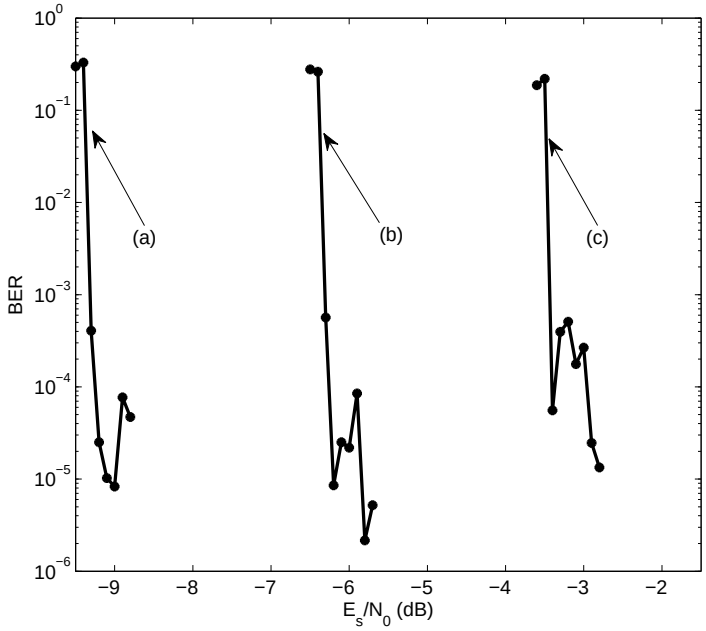

Figure 4.11: BER Performance for the low rate code cases designed in Table 4.2.

	$E_s/N_0(dB)$	d_{v1}, a_1	d_{v2}, a_2	d_{v3}, a_3	d_c	d	bits/symbol
(a)	-9.2	30, 0.5	40, 0.5		3	0.03	0.0935
(b)	-6.3	18, 0.5	20, 0.5		5	0.04	0.2055
(c)	-3.4	9, 0.5	10, 0.05	12, 0.45	8	0.05	0.4081

Table 4.2: Degree allocations of the low rate code cases in Fig. 4.10

4.2 Fading Channel

In frequency selective fading channels, there is a wide spread of the equalizer EXIT curves because of the channel variations. In some cases, the coherence time duration of the channel is too short compared with the total information length. In such cases, one has to sub-divide the information into several blocks, and encode sub-block by sub-block. One can still apply curve fitting, but the purpose of shaping the EXIT curves is to minimize *outage probability*. The question of how to determine the code parameters so that the target outage can precisely be satisfied, given fading statistics is an interesting open problem. In this thesis, we propose modulation doping and irregular repetition code techniques to approximately approach the solution to this problem. Chain simulation results are given also in this section.

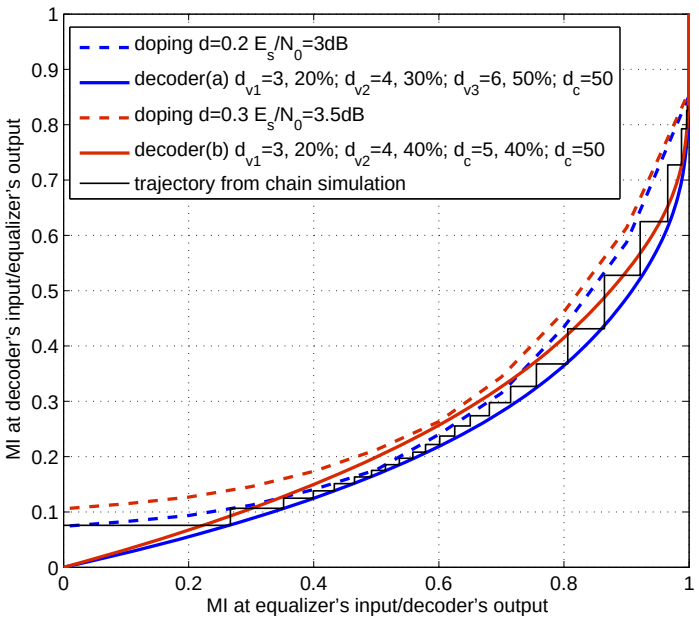

Figure 4.12: EXIT match cases of equalizer doping and irregular repetition code.

4.2.1 Doping with Irregular Repetition Code

As noted in Section 3.5, MMSE further decreases the left most point of the equalizer EXIT function, which indicatively suggests that intersection should happen at low mutual information point in many cases of the channel realization. To avoid this problem and to achieve more flexibility in code design, we introduce modulation doping, where extended mapping and Gray mapping rules are mixed in one block with a certain ratio. Fig. 4.12 shows examples of the equalizer and decoder EXIT curves, where a channel realization was drawn from the 30-path channel having equal average power delay profile. Two cases of modulation doping and two cases of the proposed code design are presented, of which parameters are summarized in the box in the figure. Result of the trajectory obtained from the chain simulation is also shown in the figure for the case with doping ratio $d = 0.2$ and decoder degree allocations $d_{v1} = 3$ $a1 = 0.2, d_{v2} = 4$ $a2 = 0.3, d_{v3} = 6$ $a3 = 0.5, d_c = 50$. It is found that the EXIT curve and trajectory are exactly matched.

Fig. 4.13 shows BER performance of the proposed system using the designed code and the doping parameters indicated in the box of Fig. 4.12. For comparison, BER performance with a rate 1/2 memory 3 non-recursive systematic convolutional coded FD SC MMSE with Gray mapping 4QAM is also shown in the figure. For all the three cases, the same static frequency selective channel realization is applied as that used in Fig. 4.12.

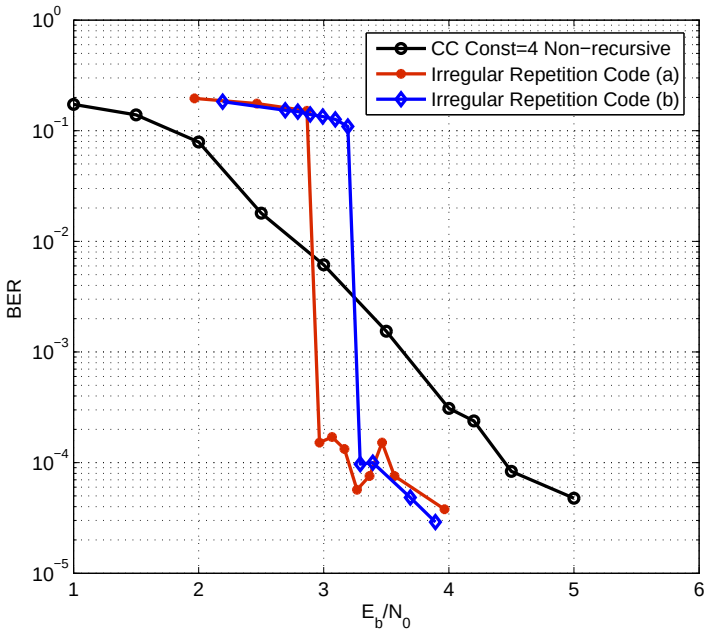

Figure 4.13: BER performance: equalization doping with irregular repetition code and equalization Gray mapping with convolutional code, by given a fixed channel realization.

4.2.2 Comparison with Conventional Technique

With the proposed technique, the most computationally heavy part is demapping, of which equation is provided in Eq. (2.25), where with 3 bits extended 4QAM ($l_{map} = 5$), the both sets S_0 and S_1 contains 16 labeling patterns; they are independently summed up in the numerator and denominator of Eq. (2.25) to calculate LLR per coded bit. With the convolutional coded turbo equalization, the Bahl-Cocke-Jelinek-Raviv (BCJR) algorithm is the most computationally heavy part, for which the Viterbi algorithm has to be performed twice (forward and backward recursion) per iteration to calculate the coded bit LLR. If we assume memory length 3 convolutional code, both S_0 and S_1 contain 8 state transition patterns and the Viterbi algorithm has to be performed twice per coded bit, resulting in 16 times per coded bit. Therefore, this comparison is fair.

It is found from the Fig. 4.13 that with the proposed system, clear turbo cliff happens at exactly the designed SNR point, while convolutional coded FD SC MMSE with Gray mapping 4QAM, no turbo cliff is observed. (For fair comparison between the codes having different code rates, E_b/N_0 is used in the figure, even though their rates are almost the same.)

From the viewpoint of outage based transmission chain design, we also generate the empirical cumulative distribution function (CDF) of BER taken from various realizations

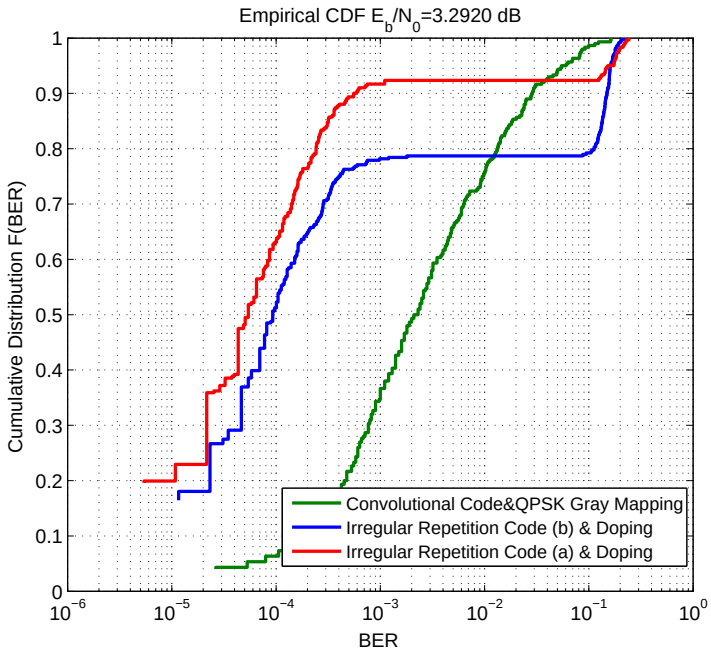

Figure 4.14: BER CDF for irregular repetition coded doping equalization and convolutional coded QPSK Gray mapping equalization, by given a fixed channel realization.

of the channel having equal average power delay profile, as shown in Fig. 4.14. At average $E_b/N_0 = 3.292dB$ ($E_s/N_0 = 3.1dB$ before the adjustment for the code rate). It is found from the figure that approximately from $BER = 5 * 10^{-4}$ to 10^{-1}, CDF of BER with the proposed system exhibits almost no increase (80%), and in the $BER > 10^{-1}$ range, the CDF curve increases to the 100% point. Obviously, the flat section corresponds to the turbo cliff range, i.e. turbo cliff happens with 80% of the probability of channel realizations when average $E_s/N_0 = 3.1dB$. In the $BER < 5 * 10^{-4}$ range, CDF gradually increases, which corresponds to the asymptotic BER range. On the contrary, CDF with rate 1/2 convolutional coded FD SC MMSE with Gray mapping 4QAM only monotonically increases in entire range of BER. This indicates that since the variation of the equalizer EXIT curve is very large, intersection of the EXIT curves happen in a wide range of mutual information, even though the average E_s/N_0 is fixed at $3.1dB$, resulting in large variation in BER. Furthermore, $BER < 10^{-2}$ happens with larger probability with the proposed system than the rate 1/2 convolutional coded FD SC MMSE, which means that with the proposed scheme, the EXIT curves of the equalizer and the decoder are well matched in a variety of channel realizations, and mutual information close to 1 can be achieved with higher probability than rate 1/2 convolutional coded FD SC MMSE with Gray mapping 4QAM.

Chapter 5

Conclusions and Outlook

Conclusions

In this work, extended mapping/FD SC MMSE equalization jointly designed with check node assisted irregular repetition code has been proposed to optimize the performance of BICM-ID transmission system. This approach is firstly investigated in AWGN channel to better observe its properties, and further extended to frequency selective fading channel with the aim of making the outage based transmission feasible. The main contributions that have been achieved in the course of this work are summarized as follows:

- Extended mapping scheme enables flexible adaptation to the channel conditions without requiring prohibitively large computational complexity by adjusting the labeling length while keeping the constellation diagram constant. This brings advantages to practical systems in avoiding switching the constellation diagram and the impairment of high order modulations. Therefore, extended mapping can significantly reduce the hardware complexity compared to using higher order modulation schemes.

- To achieve high power and spectral efficiencies, check node assisted irregular repetition code is constructed to minimize the area between demapper and channel decoder EXIT functions while without getting intersect before reaching a close to MI=1 point. The structure of this code is extremely simple and the complexity is low. There is no iteration needed in this decoder itself. The turbo cliff and BER floor are further flexibly controlled in given desired SNR values, by carefully choosing the irregular degree allocations. Moreover, doping modulation helps to realize very low rate code design. Yet, the method to obtain the optimal degree allocations has not been developed systematically.

- The proposed technique makes it possible to compress the variation of EXIT curves due to the channel fading variation. Hence, it provides a practical solution to the

outage-based transmission chain optimization. Comparing with the conventional technique, which is convolutional coded FD SC MMSE with Gray mapping, the complexity is almost equivalent, but performance can be significantly improved.

Outlook

In the course of this work, several problems have appeared or been left unsolved, among which the following are of particular interest:

- The degree allocation of check node assisted irregular repetition code could be systematically achieved, by recognizing that the problem can be formulated in a mathematical way with which some numerical tools/algorithms such as genetic algorithms can be used.

- Even though the outage-based transmission is made possible by the proposed system, it does not mean that the adaptive transmission is unnecessary. In fact, it does eliminate the necessity of the instantaneous power control and code parameter optimization, however, if the EXIT variation is too large, still we cannot expect clear BER threshold. Therefore, a practical approach to outage-based adaptive transmission chain control in broadband single carrier signaling with turbo equalization has to be developed.

- Technological bases towards optimal design of PHY-and-MAC layers for point-to-point communications have already been almost entirely researched in general, and recently in wireless communication research community, major focus has been directed to more complex network structures, such as multi-hop communications, distributed source and channel coding, relaying, and multiple access/broadcasting channel coding techniques, for all of which theoretical basis is the network information theory. It may be possible to further extend and apply these techniques to the scenarios having more complicated network structures.

Appendix

A. FD SC MMSE algorithm

A priori information is provided by decoder in the form of LLR λ. We define the soft estimate of the k-th transmitted symbol as the expectation of $x(k), \mathbf{E}\{x(k)\}$, as

$$\hat{x}(k) = \sum_{x_i \in \Phi} x_i \cdot P(x(k) = x_i), \tag{a}$$

with

$$P(x(k) = x_i) = \frac{1}{2^{l_{map}}} \prod_{m=1}^{l_{map}} \left(1 + (1 - 2u_m(x_i)) \cdot tanh\left\{\frac{\lambda[u_m(x_i)]}{2}\right\}\right), \tag{b}$$

where $u_m(x_i)$ is the m-th bit of the symbol x_i.

The vector of symbol estimate $\hat{\mathbf{x}} = [\hat{x}(1), \cdots, \hat{x}(N)]^T$ given by (17) is used to construct the estimate of the received signal $\mathbf{y}$ by suppressing the residual error $\tilde{\mathbf{y}}$. The residual error of the k-th symbol is given by

$$\tilde{\mathbf{y}}(k) = \mathbf{y} - \mathbf{H}^c\tilde{\mathbf{x}} + \mathbf{h}(k)\hat{x}(k), \tag{c}$$

where $\mathbf{h}(k)$ is a k-th column of the channel matrix $\mathbf{H}^c$ of (4). The weight for MMSE filtering is then determined such that

$$\mathbf{w}(k) = \arg\min_{\mathbf{w}^H(k)} \left|\mathbf{w}^H(k)\tilde{\mathbf{y}}(k) - x(k)\right|^2, \tag{d}$$

to obtain the block-wise equalizer output

$$\mathbf{z} = (\mathbf{I}_N + \mathbf{\Gamma X})^{-1}\left[\mathbf{\Gamma}\hat{\mathbf{x}} + \mathbf{F}^H\mathbf{\Psi F}\hat{\mathbf{y}}\right], \tag{e}$$

where

$$\mathbf{\Gamma} = \gamma \cdot \mathbf{I}, \tag{f}$$

with

$$\gamma = \frac{1}{N} tr\left[\mathbf{\Xi}\left(\mathbf{\Xi}\mathbf{\Delta}\mathbf{\Xi}^H + \sigma_N^2 \mathbf{I}_k\right)^{-1}\mathbf{\Xi}\right], \tag{g}$$

$$\mathbf{X} = diag\left[|\hat{x}|^2\right], \tag{h}$$

$$\mathbf{\Psi} = \mathbf{\Xi}^H\left(\mathbf{\Xi}\mathbf{\Delta}\mathbf{\Xi}^H + \sigma_N^2 \mathbf{I}\right)^{-1}, \tag{i}$$

and $\mathbf{\Delta} = \mathbf{F}\mathbf{\Lambda}\mathbf{F}^H$ is the frequency domain of residual symbol error covariance, where

$$\mathbf{\Lambda} = E\left[\mathbf{x} - \hat{\mathbf{x}}\right] = diag\left\{E\left[|\mathbf{x}|^2\right] - \left|\hat{\mathbf{x}}^2\right|\right\}. \tag{j}$$

To compute the extrinsic LLR used in (8), the equalizer output is approximated as Gaussian distribution $\mathbf{z} \sim N\left(\mu_{EQ}, \sigma_{EQ}\right)$, where

$$\mu_{EQ} = \gamma\left(1 + \gamma\hat{x}\right)^{-1} \tag{k}$$

$$\sigma_{EQ}^2 = \mu_{EQ}\left(1 - \mu_{EQ}\right). \tag{l}$$

B. Mapping

Standard Mapping

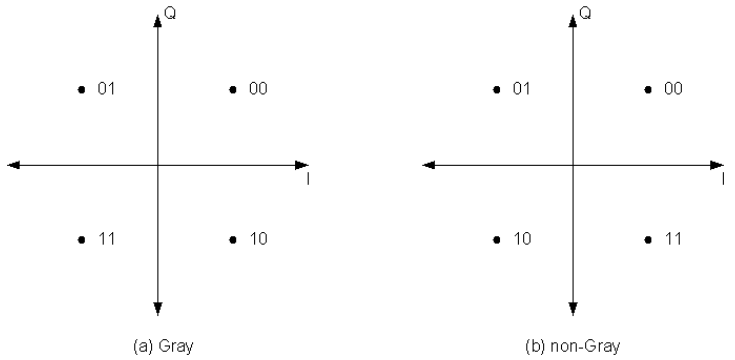

Figure A: 4QAM standard mapping.

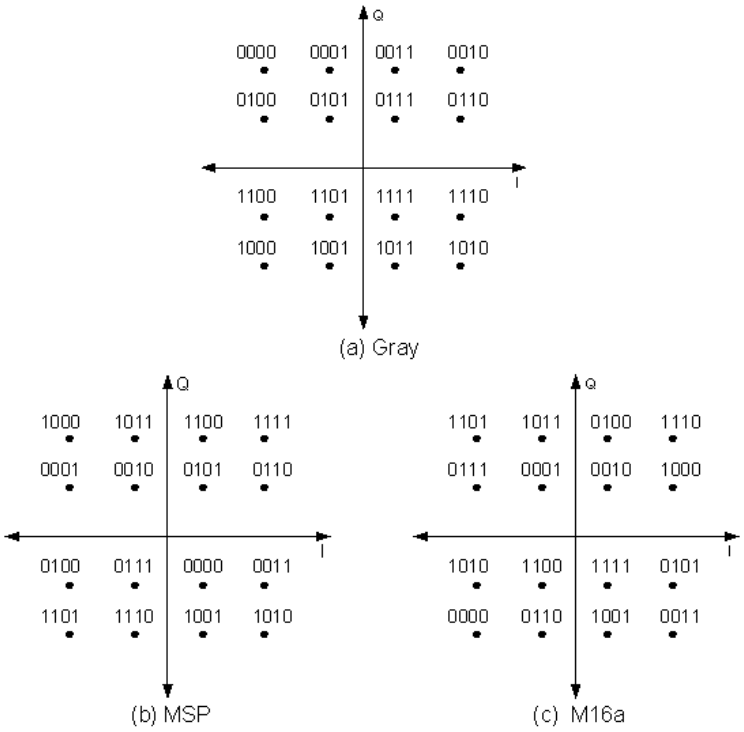

Figure B: 16QAM standard mapping [1].

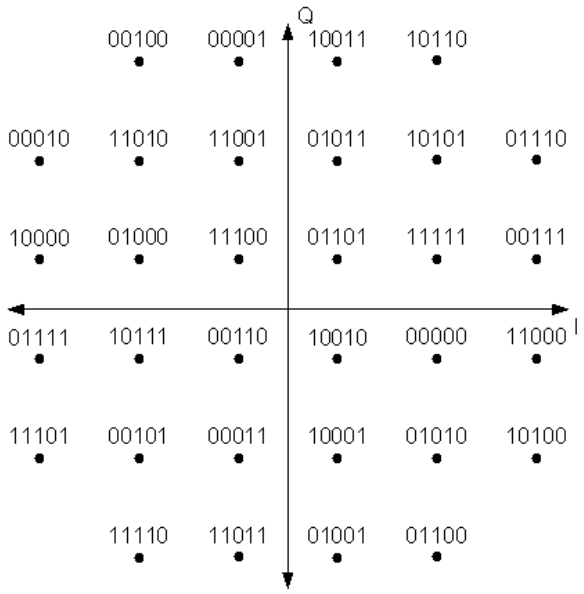

Figure C: 32QAM standard mapping M32a [1].

Extended Mapping

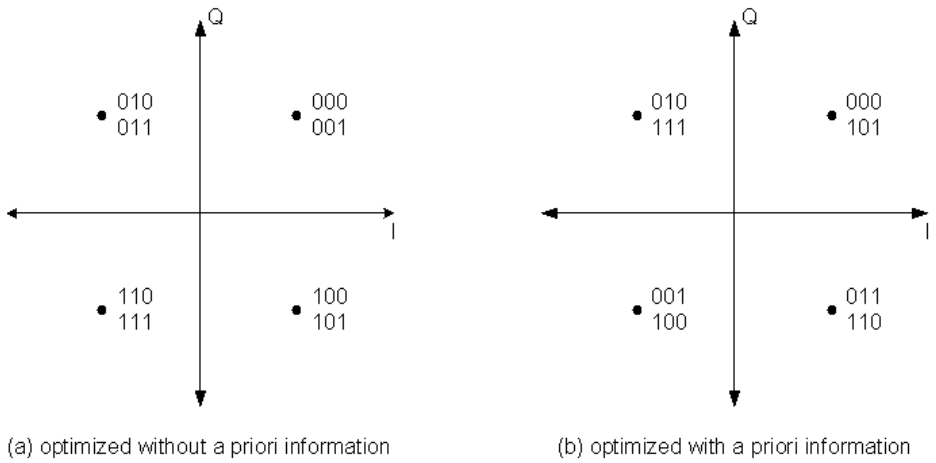

Figure D: 4QAM extended mapping $l_{map} = 3$.

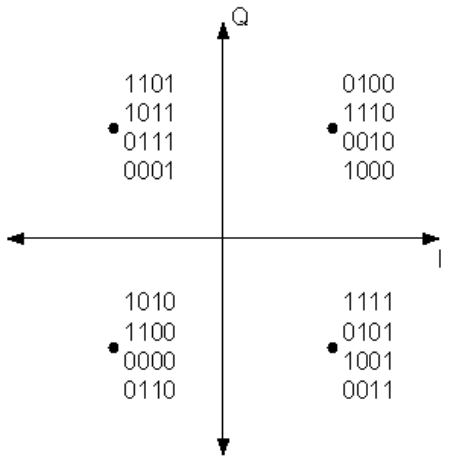

Figure E: Extended mapping 4QAM $l_{map} = 4$ optimized with a priori information.

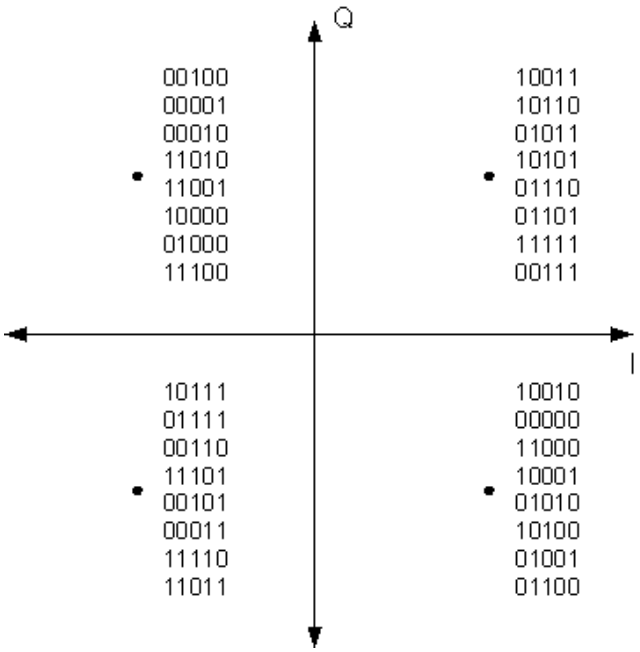

Figure F: Extended mapping 4QAM $l_{map} = 5$ optimized with a priori information.

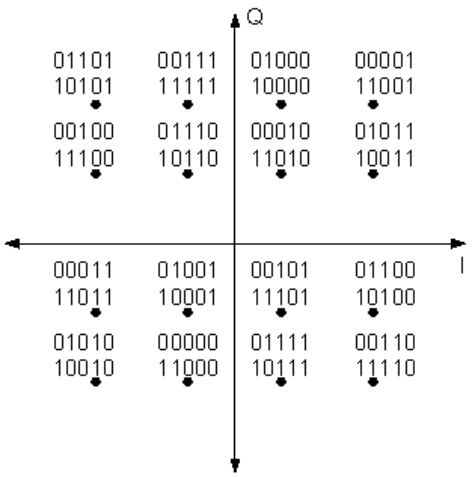

Figure G: Extended mapping 16QAM $l_{map} = 5$ optimized with a priori information [2].

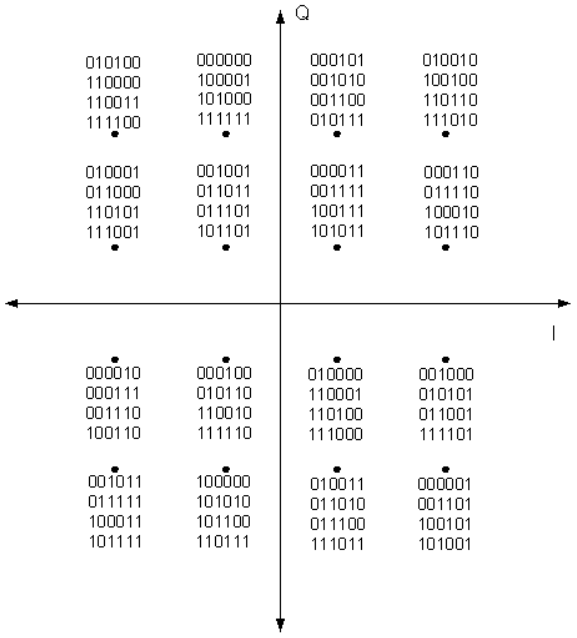

Figure H: Extended mapping 16QAM $l_{map} = 6$ optimized with a priori information [2].

Abbreviations and Notation

AWGN	additive white Gaussian noise
BCJR	MAP algorithm by Bahl, Cocke, Jelinek, Raviv
BER	bit error rate
BICM	bit-interleaved coded modulation
BICM-ID	bit-interleaved coded modulation with iterative detection
CDF	cumulative distribution function
CP	cyclic prefix
EM	extended mapping
EXIT	extrinsic information transfer
FD SC MMSE	frequency domain soft cancelation minimum mean square error
ISI	inter-symbol interference
LDPC	low-density parity-check
LLR	log-likelihood ratio
MAP	maximum a posteriori probability
MI	mutual information
MLC	multilevel codes
MSP	modified set partitioning mapping
PHY-and-MAC	physical-and-medium access
QAM	quadrature amplitude modulation
SNR	signal-to-noise power ratio
TCM	trellis-coded modulation

$(\hat{\cdot})$	estimate of the argument
$(\cdot)^{-1}$	inverse of the argument
$(\cdot)^{H}$	Hermitian(transposed complex conjugation) of a matrix
$(\cdot)^{T}$	transpose of a vector or matrix
$\lvert\cdot\rvert$	absolute value
$\langle\cdot\rangle$	expectation of the argument
$\mathbb{C}$	field of the complex numbers
$diag\,(\cdot)$	diagonal matrix with vector elements on its diagonal components
exp	exponential calculation to base e
$erfc\,(\cdot)$	complementary error function
$E\,\{\cdot\}$	expectation of a random variable
$J\,(\cdot)$	J-function
$ln\,(\cdot)$	natural logarithm (to base e)
$\log_2\,(\cdot)$	natural logarithm (to base 2)
max	maximum value
$\mathcal{N}\,(\cdot,\cdot)$	Gaussian distribution
$\sum\boxplus$	boxplus operation

$\mathbb{A}$	area under the EXIT function
B	coded bits
$circ\,(\cdot))$	operator for making circulant matrix
C	capacity
d	doping ratio
d_c	check node degree
d_E	Euclidean distance
d_v	variable node degree
E_b/N_0	bit-wise signal to noise ratio
$f\,(\cdot)$	EXIT curve function
$\mathbf{F}$	discrete Fourier matrix
h	flat fading channel gain
$\mathbf{h}$	frequency selective fading channel gain vector
$H\,(\cdot)$	entropy of the variable
$\mathbf{H}$	fading channel matrix with Toeplitz structure
$\mathbf{H}^c$	circulant matrix
$I\,(\cdot;\cdot)$	mutual information
I_a	a priori information
$I_{a,v}$	a priori information to variable node
$I_{a,cnd}$	a priori information to check node
$I_{a,dec}$	a priori information to decoder
$I_{a,dem}$	a priori information to demapper
I_e	extrinsic information
$I_{e,v}$	extrinsic information output from variable node

$I_{e,cnd}$	extrinsic information output from check node
$I_{e,dec}$	extrinsic information output from decoder
$I_{e,dem}$	extrinsic information output from demapper
$\mathbf{I}$	identity matrix
l_c	constraint length for convolutional code
l_{map}	labeling length
L	number of the paths in fading channel
$L(\cdot)$	log-likelihood ratio
L_a	a priori LLR
$L_{a,cnd}$	a priori LLR to check node
L_c	channel LLR
L_e	extrinsic LLR
$L_{e,cnd}$	extrinsic LLR output from check node
L_p	a posteriori LLR
M	number of constellation points
$\mathbf{n}$	zero mean complex AWGN vector
N	number of bits in one block
$N_N(\cdot,\cdot)$	distance spectrum
$\bar{N}(\cdot)$	averaged distance spectrum
$p(\cdot)$	probability density function of the random variable
P	number of sub-blocks for a transmitted block
$P(\cdot)$	probability of the variable
r_c	code rate
s	symbols in constellation diagram
S	set of the symbol labels
$Toepl(\cdot)$	operator that makes Toeplitz matrix from a vector
u_k	a binary random variable
$v(t)$	AWGN complex symbol in continuous time
$\mathbf{v}$	Gaussian noise vector in continuous time
$x(\cdot)$	transmitted complex symbol
$\mathbf{x}$	transmitted symbol block/vector
$y(\cdot)$	received complex symbol
$\mathbf{y}$	received symbol block/vector
$\mathbf{z}$	soft symbol vector from equalizer calculation
μ_{EQ}	mean of equalizer output LLR
μ_L	mean of LLR
μ_{EQ}	mean of equalizer output LLR
σ_t^2	Gaussian noise variance in continuous time domain
σ_N^2	Gaussian noise variance
σ_{EQ}^2	variance of equalizer output LLR
σ_L^2	variance of LLR
Φ	mapping rule
χ	constellation diagram
Ξ	frequency domain channel matrix

Bibliography

[1] F. Schreckenbach, N. Gortz, J. Hagenauer, and G. Bauch, "Optimized symbol mappings for bit-interleaved coded modulation with iterative decoding," in *Proc. of the IEEE GLOBECOM*, 2003.

[2] P. Henkel, "Extended Mappings for Bit-Interleaved Coded Modulation," in *17th IEEE International Symposium on Personal, Indoor and Mobile Radio Communications (PIMRC).*

[3] C. Shannon, "The mathematical theory of communication," *Bell Syst. Tech. J*, vol. 27, pp. 379–423, 1948.

[4] C. Berrou, A. Glavieux, and P. Thitimajshima, "Near shannon limit error correcting coding and decoding: Turbo codes." *Proc. of IEEE International Conference on Communications (ICC). Geneva, Switzerland*, pp. 1064–1070, 1993.

[5] J. Hagenauer, "The turbo principle: Tutorial introduction and state of the art," in *Proc. International Symposium on Turbo Codes and Related Topics*, 1997, p. 111.

[6] J. Massey, "Coding and modulation in digital communications," in *International Zurich Seminar on Digital Communications, 3 rd, Zurich, Switzerland; United States; 12-15 Mar.* New York, Institute of Electrical and Electronics Engineers, Inc., 1974.

[7] G. Ungerboeck, "Channel coding with multilevel/phase signals," *IEEE Transactions on Information Theory*, vol. 28, no. 1, pp. 55–67, 1982.

[8] H. Imai and S. Hirakawa, "A new multilevel coding method using error-correcting codes," *IEEE Transactions on Information Theory*, vol. 23, no. 3, pp. 371–377, 1977.

[9] U. Wachsmann, R. Fischer, and J. Huber, "Multilevel codes: Theoretical concepts and practical design rules," *IEEE Transactions on Information Theory*, vol. 45, no. 5, pp. 1361–1391, 1999.

[10] G. Caire, G. Taricco, and E. Biglieri, "Bit-interleaved coded modulation," *IEEE Transactions on Information Theory*, vol. 44, no. 3, pp. 927–946, 1998.

[11] X. Li and J. Ritcey, "Bit-interleaved coded modulation with iterative decoding," *IEEE Communications Letters*, vol. 1, no. 6, pp. 169–171, 1997.

[12] J. Hagenauer, "The EXIT chart-introduction to extrinsic information transfer in iterative processing," in *Proc. 12th Europ. Signal Proc. Conf (EUSIPCO)*, 2004.

[13] S. ten Brink, "Convergence behavior of iteratively decoded parallel concatenated codes," *IEEE Transactions on Communications*, vol. 49, no. 10, pp. 1727–1737, 2001.

[14] P. Henkel, "Doping of Extended Mappings for Signal Shaping," in *IEEE 65th Vehicular Technology Conference, 2007. VTC2007-Spring*, 2007, pp. 1851–1855.

[15] K. Kansanen and T. Matsumoto, "An Analytical Method for MMSE MIMO Turbo Equalizer EXIT Chart Computation," *IEEE Transactions on Wireless Communications*, vol. 6, pp. 59–63, 2007.

[16] L. Hanzo, T. Liew, and B. Yeap, *Turbo coding, turbo equalisation, and space-time coding for transmission over fading channels*. John Wiley, 2002.

[17] J. Hagenauer, E. Offer, and L. Papke, "Iterative decoding of binary block and convolutional codes," *IEEE Transactions on Information Theory*, vol. 42, no. 2, pp. 429–445, 1996.

[18] S. Ten Brink, J. Speidel, and R. Yan, "Iterative demapping and decoding for multilevel modulation," in *IEEE Global Telecommunications Conference, 1998. GLOBECOM 98. The Bridge to Global Integration*, vol. 1, 1998.

[19] K. Zeger and A. Gersho, "Pseudo-gray coding," *IEEE Transactions on communications*, vol. 38, no. 12, pp. 2147–2158, 1990.

[20] F. GRAY, "Pulse code communication," 1953, uS Patent 2,632,058.

[21] A. Chindapol and J. Ritcey, "Design, analysis and performance evaluation for BICM-ID with square QAM constellations in Rayleigh fading channels," *IEEE Journal on Selected Areas in Communications*, vol. 19, no. 5, pp. 944–957, 2001.

[22] S. ten Brink, "Code doping for triggering iterative decoding convergence," in *2001 IEEE International Symposium on Information Theory. Proceedings*, 2001.

[23] F. Schreckenbach and G. Bauch, "Adaptive bit-interleaved coded irregular modulation," in *Proc. 14th IST Mobile & Wireless Communications Summit*, 2005, pp. 1332–1336.

[24] ——, "Bit-interleaved coded irregular modulation," *European Transactions on Telecommunications*, vol. 17, no. 2, pp. 269–282, 2006.

[25] S. Lin and D. J. Costello, *Error Control Coding, Second Edition*. Upper Saddle River, NJ, USA: Prentice-Hall, Inc., 2004.

[26] P. Robertson, E. Villebrun, and P. Hoeher, "A comparison of optimal and sub-optimal MAP decoding algorithms operating in the log domain," in *Communications, 1995. ICC '95 Seattle, 'Gateway to Globalization', 1995 IEEE International Conference on*, vol. 2, Jun 1995, pp. 1009–1013.

[27] T. Richardson and R. Urbanke, "The capacity of low-density parity-check codes under message-passing decoding," *IEEE Transactions on Information Theory*, vol. 47, no. 2, pp. 599–618, 2001.

[28] T. Richardson, M. Shokrollahi, and R. Urbanke, "Design of capacity-approaching irregular low-density parity-check codes," *IEEE Transactions on Information Theory*, vol. 47, no. 2, pp. 619–637, 2001.

[29] S. Chung, T. Richardson, R. Urbanke *et al.*, "Analysis of sum-product decoding of low-density parity-check codes using a Gaussian approximation," *IEEE Transactions on Information Theory*, vol. 47, no. 2, pp. 657–670, 2001.

[30] D. Divsalar, S. Dolinar, and F. Pollara, "Low complexity turbo-like codes," in *Proc. Int. Symp. Turbo Codes*, 2000.

[31] H. El Gamal and A. Hammons, "Analyzing the turbo decoder using the Gaussian approximation," *IEEE Transactions on Information Theory*, vol. 47, no. 2, pp. 671–686, 2001.

[32] S. ten Brink, "Rate one-half code for approaching the Shannon limit by 0.1 dB," *Electron. Lett*, vol. 36, no. 15, pp. 1293–1294, 2000.

[33] M. Tuchler, S. Ten Brink, and J. Hagenauer, "Measures for tracing convergence of iterative decoding algorithms," in *Proc. 4th IEEE/ITG Conf. on Source and Channel Coding*, 2002, pp. 53–60.

[34] T. Cover and J. Thomas, *Elements of information theory*. Wiley, 2006.

[35] A. Ashikhmin, G. Kramer, and S. Ten Brink, "Extrinsic information transfer functions: model and erasure channel properties," *IEEE Transactions on Information Theory*, vol. 50, no. 11, pp. 2657–2673, 2004.

[36] P. Hoeher, I. Land, and U. Sorger, "Log-likelihood values and Monte Carlo simulation-some fundamental results," in *2nd International Symposium on Turbo Codes and Related Topics*, 2000, pp. 43–46.

[37] F. Brannstrom, L. Rasmussen, and A. Grant, "Convergence analysis and optimal scheduling for multiple concatenated codes," *IEEE Transactions on Information Theory*, vol. 51, no. 9, pp. 3354–3364, 2005.

[38] S. ten Brink, "Code characteristic matching for iterative decoding of serially concatenated codes," *Annals of Telecommunications*, vol. 56, no. 7, pp. 394–408, 2001.

[39] S. ten Brink, G. Kramer, and A. Ashikhmin, "Design of low-density parity-check codes for modulation and detection," *IEEE Transactions on Communications*, vol. 52, no. 4, pp. 670–678, 2004.

[40] S. ten Brink, "Exploiting the chain rule of mutual information for the design of iterative decoding schemes," in *39th Allerton Conference on Communications, Control and Computing, Monticello, Urbana-Champaign*, 2001.

[41] J. Proakis and M. Salehi, *Digital communications*. McGraw-hill New York, 1995.